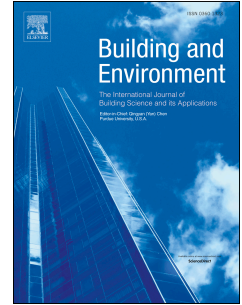


Journal Pre-proof

Impact of building density on natural ventilation potential and cooling energy saving across Chinese climate zones

Xiaoxiong Xie, Zhiwen Luo, Sue Grimmond, Ting Sun



PII: S0360-1323(23)00648-0

DOI: <https://doi.org/10.1016/j.buildenv.2023.110621>

Reference: BAE 110621

To appear in: *Building and Environment*

Received Date: 1 May 2023

Revised Date: 10 July 2023

Accepted Date: 15 July 2023

Please cite this article as: Xie X, Luo Z, Grimmond S, Sun T, Impact of building density on natural ventilation potential and cooling energy saving across Chinese climate zones, *Building and Environment* (2023), doi: <https://doi.org/10.1016/j.buildenv.2023.110621>.

This is a PDF file of an article that has undergone enhancements after acceptance, such as the addition of a cover page and metadata, and formatting for readability, but it is not yet the definitive version of record. This version will undergo additional copyediting, typesetting and review before it is published in its final form, but we are providing this version to give early visibility of the article. Please note that, during the production process, errors may be discovered which could affect the content, and all legal disclaimers that apply to the journal pertain.

© 2023 Published by Elsevier Ltd.

1 **Impact of building density on natural ventilation potential and cooling energy saving**
 2 **across Chinese climate zones**

3 Xiaoxiong Xie ^a, Zhiwen Luo ^{b*}, Sue Grimmond ^c, Ting Sun ^d

4 ^a School of the Built Environment, University of Reading, United Kingdom

5 ^b Welsh School of Architecture, Cardiff University, United Kingdom

6 ^c Department of Meteorology, University of Reading, United Kingdom

7 ^d Institute for Risk and Disaster Reduction, University College London, United Kingdom

8

9 Word count of abstract: 199

10 Word count of text: 7792

11 *Corresponding author: Prof Zhiwen Luo; Email: LuoZ18@Cardiff.ac.uk

12 **Abstract**

13 Natural ventilation is an energy-efficient approach to reduce the need for mechanical
 14 ventilation and air conditioning in buildings. However, traditionally weather data for building
 15 energy simulation are obtained from rural areas, which do not reflect the urban
 16 micrometeorological conditions. This study combines the Surface Urban Energy and Water
 17 Balance Scheme (SUEWS) and EnergyPlus to predict natural ventilation potential (NVP) and
 18 cooling energy saving in three idealised urban neighbourhoods with different urban densities
 19 in five Chinese cities of different climate zones. SUEWS downscales the meteorological
 20 inputs required by EnergyPlus, including air temperature, relative humidity, and wind speed
 21 profiles. The findings indicate that NVP and cooling energy saving differences between
 22 urban and rural areas are climate- and season-dependent. During summer, the urban-rural
 23 differences in natural ventilation hours are -43% to 10% (cf. rural) across all climates, while
 24 in spring/autumn, they range from -7% to 36%. The study also suggests that single-sided
 25 ventilation can be as effective as cross ventilation for buildings in dense urban areas. Our
 26 findings highlight the importance of considering local or neighbourhood-scale climate when

27 evaluating NVP. We demonstrate a method to enhance NVP prediction accuracy in urban
 28 regions using EnergyPlus, which can contribute to achieving low-carbon building design.

29

30 **Keywords:** Natural ventilation, urban climate, land surface model, EnergyPlus, climate zone

31 **Nomenclature**

32	A	Effective opening area (m ²)
33	C _d	Discharge coefficient of opening
34	C _p	Wind pressure coefficient
35	g	Gravitational acceleration (m s ⁻²)
36	h _{opening}	Height of opening (m)
37	P _w	Wind pressure (Pa)
38	Q _{saving}	Cooling energy saving (J)
39	T	Air temperature (°C)
40	U	Wind speed (m s ⁻¹)
41	V	Ventilation rate (m ³ s ⁻¹)
42	α	Wind profile exponent
43	δ	Height where a constant mean gradient wind speed is assumed to occur (m)
44	λ _p	Plan area fraction
45	ρ ₀	Outdoor air density (kg m ⁻³)
46		
47	subscripts	
48	b	Buoyancy-driven
49	w	Wind-driven
50	ref	Reference condition at the meteorological station

51 **1. Introduction**

52 The Paris Agreement calls on countries to cut carbon emissions to meet the target of limiting
 53 global warming to preferably 1.5 °C compared to pre-industrial levels (UN, 2015). In 2019,
 54 carbon emissions from the operation of buildings accounted for 28% of total global energy-
 55 related carbon emissions (UNEP, 2020). Although in China building operation contributes to
 56 21.6 % of national carbon emissions (CABEE, 2021), China's building energy consumption is
 57 expected to continue to rise with urbanisation and climate change. Thus, it is important but
 58 challenging to improve energy efficiency.

59 Natural ventilation is a key passive cooling strategy used to achieve low-carbon building
 60 design. It reduces energy consumption, and improves occupants' health, comfort, and
 61 productivity (Emmerich et al., 2001). As the effectiveness of natural ventilation depends on
 62 the outdoor weather conditions, these impacts need to be assessed.

63 Natural ventilation potential (NVP) is defined as the possibility (or probability) of achieving
64 acceptable indoor thermal comfort and air quality through natural ventilation alone (Luo et
65 al., 2007). Although studied worldwide using different methods and metrics (Table 1),
66 assessing NVP can be difficult due to its sensitivity to factors such as weather, climate,
67 building design, and the surrounding environment (Yin et al., 2010). Current methods can be
68 generally categorised into climate-based and building simulation approaches (Wang and
69 Malkawi, 2019).

70 Climate-based approaches provide broad geographic NVP variations using outdoor air
71 temperature and wind speed (Wang and Malkawi, 2019), for use in the early design stage
72 when detailed building information is unavailable (outdoor data analysis, Table 1). For
73 example, Chen et al.'s (2017) global analysis using typical meteorological year (TMY) data
74 found temperate climates (e.g. subtropical highland, Mediterranean) tend to have larger NVP
75 compared to more extreme climates (e.g. tropical, subarctic). Humidity has also been
76 identified as being important when assessing NVP in hot-humid climates (Causone, 2016).

77 Using building energy simulation tools (e.g. EnergyPlus (U.S. Department of Energy, 2020a),
78 TRNSYS (2009), DeST (Yan et al., 2008), IES-VE (Integrated Environmental Solutions,
79 2018)) NVP assessments can account for building design elements (building simulation,
80 Table 1) including impacts such as the internal heat gain, building envelope, occupancy
81 schedule and ventilation pattern. In comparison to climate-based approaches, building
82 simulations can mitigate uncertainties arising from building location and design. Numerous
83 studies (Anđelković et al., 2016; Fumo et al., 2010; Lam et al., 2014; Royapoor and Roskilly,
84 2015; Ryan and Sanquist, 2012) have demonstrated the capability of building energy
85 simulation tools to accurately model indoor thermal environments (hourly biases $< 10\%$ for
86 energy consumption and $< 1.5\text{ }^{\circ}\text{C}$ for indoor air temperature), given that detailed and precise

87 input data are available. Therefore, it is crucial to use appropriate weather data inputs for
 88 building energy simulation purposes (Hensen, 1999).

89 Originally (and typically) building energy simulation tools treat buildings as being isolated,
 90 using weather data input acquired from meteorological stations located in open country.

91 However, the climate in urban areas is known to differ from surrounding rural areas due to
 92 various aspects of the urban environment potentially affecting natural ventilation (Oke et al.,

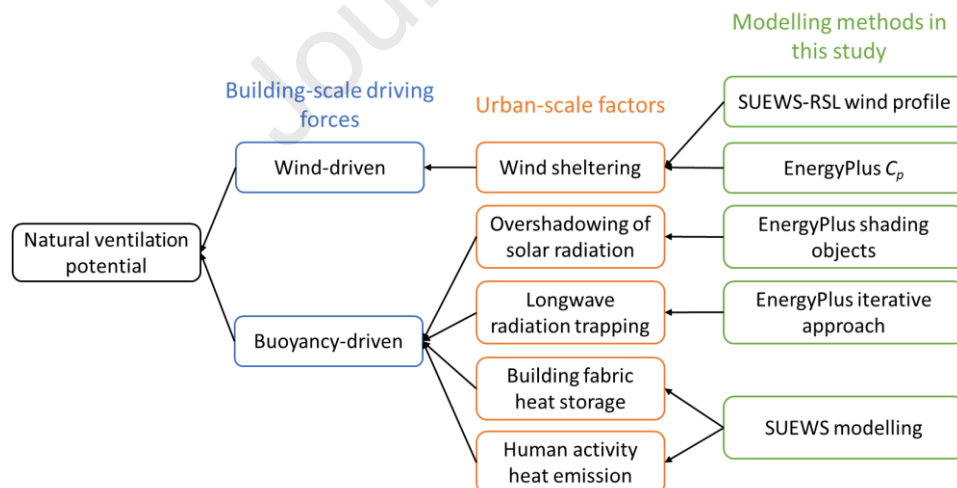
93 2017a), as shown in Fig. 1. Under wind-driven ventilation conditions the airflow pattern is
 94 influenced by surrounding buildings modifying the wind pressure on building facades (van

95 Hooff and Blocken, 2010; Yang et al., 2008; Zhang et al., 2005). Whilst buoyancy-driven

96 ventilation is affected by warmer outdoor air temperatures caused by the canopy layer urban
 97 heat island effect (WMO, 2023), which is a result of the building fabric affecting heat storage

98 and waterproofing (Grimmond et al., 1986; Grimmond and Oke, 1999a), anthropogenic heat
 99 release from human activities (Allen et al., 2011; Sailor, 2011), trapped longwave radiation

100 (Xie et al., 2022) and reduced wind speed (WMO, 2023).



101
 102
 103
 104
 105

Fig. 1. Factors influencing natural ventilation potential in urban areas and the modelling methods used in this study. C_p : wind pressure coefficient.

106 Considering these impacts, employing a traditional approach that relies on rural weather data
 107 for building simulations in urban environments can introduce large biases in building energy

108 performance, indoor thermal environment and natural ventilation rate. Previous studies
109 explored these biases resulting from neglecting the impacts of urban factors. Neglecting
110 increases in urban air temperature can cause biases of up to 11% in building energy
111 consumption (Boccalatte et al., 2020; Kamal et al., 2021; Liu et al., 2017; Magli et al., 2015).
112 For buildings situated in dense neighbourhoods (with a building plan area fraction (λ_P) of
113 0.6), neglecting the wind sheltering effect can overpredict the natural ventilation rate by as
114 much as 19% (Xie et al., 2023), while overlooking the effect of inter-building longwave
115 radiative exchange can underpredict the annual cooling energy by up to 17% (Xie et al.,
116 2022). Such biases in natural ventilation rates and indoor thermal environments can influence
117 the NVP assessment.

118 Some studies have accounted for urban climate when assessing NVP, with most using
119 computational fluid dynamic (CFD) models (Table 1) to obtain air flow (Toparlar et al.,
120 2017). However, CFD methods are dependent on the meteorological boundary conditions and
121 the building morphology details, and their high computational costs make them unsuitable for
122 long-term and large-scale simulations. Long-term modelling using EnergyPlus has accounted
123 for urban climate, by modifying weather data using a simple urban heat island scenario that
124 considers the air temperature only, so natural ventilation cooling energy savings can be
125 simulated (Ramponi et al., 2014). However, their urban heat island (UHI) prediction only
126 considers a fixed UHI magnitude, which does not account for neighbourhood density (or
127 building plan area fraction), and thus may not fully represent the local climate. Tong et al.
128 (2017) accounted for local atmospheric conditions on NVP for super high-rise buildings
129 using Monin-Obukhov similarity theory (MOST) approach. However, MOST applies in the
130 inertial sublayer (a layer that begins 2 to 5 times above the mean canopy height) if present but
131 not in the roughness sublayer (Grimmond and Oke, 1999b; Theeuwes et al., 2019). Also, the
132 analysis did not consider inter-buildings impacts such as radiation. In summary, the

133 comprehensive consideration of all urban impacts shown in Fig. 1 when assessing NVP is
134 currently limited in the existing literature.

135 To better account for urban impacts on NVP, in this study we propose a multi-scale
136 modelling scheme by combining the urban land surface model Surface Urban Energy and
137 Water Balance Scheme (SUEWS) (Järvi et al., 2011) and the building simulation tool
138 EnergyPlus (U.S. Department of Energy, 2020a).

139 SUEWS uses commonly available surface characteristics and climate forcing data to simulate
140 energy and water fluxes and derive local-scale environmental parameters (Järvi et al., 2011;
141 Ward et al., 2016). It addresses the limitations of previous urban land surface models
142 (Grimmond et al., 2011, 2010) by specifically addressing the better representation of latent
143 heat flux and incorporating multiple sub-models to enhance accuracy (Järvi et al., 2011). The
144 performance of SUEWS has been extensively evaluated in diverse global climates (see Table
145 3 of Lindberg et al. (2018); Table 1 of Sun and Grimmond (2019)), demonstrating its
146 acceptable accuracy. Notably, Tang et al. (2021) evaluated SUEWS air temperature profile
147 against observations at a central London site, considering two different heights above ground,
148 and reported mean absolute errors (MAEs) of less than 1 °C. Furthermore, Theeuwes et al.
149 (2019) compared the wind profile modelled with the modified MOST approach embedded in
150 SUEWS with observations in Basel and Gothenburg, reporting MAEs ranging from 0.15 to
151 0.5 m s⁻¹ at roof level. Applications of SUEWS in various urban environments worldwide
152 have provided valuable insights. Researchers have used SUEWS to investigate the impacts of
153 urbanisation on local climate (e.g. Fernández et al., 2021; Lindberg et al., 2020; Rafael et al.,
154 2020) and building energy performance (Tang et al., 2021), assess the performance of green
155 infrastructure (e.g. Havu et al., 2022; Wiegels et al., 2021), and analyse the effectiveness of
156 different heat mitigation strategies (e.g. Augusto et al., 2020; Ward and Grimmond, 2017).

157 The open-source U.S. Department of Energy (2020a) EnergyPlus building energy simulation
158 tool is one of the most widely used, and can be used for assessing natural ventilation potential
159 (Table 1). Following extensive evaluation, EnergyPlus has been shown to accurately model
160 the indoor thermal environment and natural ventilation given accurate and detailed input
161 information. For example, Royapoor and Roskilly (2015) report a calibrated EnergyPlus
162 model can predict annual hourly indoor air temperatures with an accuracy of ± 1 °C for 93.2%
163 of the time. Whilst, from comparing EnergyPlus Airflow Network (AFN) model results to
164 experimental data Johnson et al. (2012) conclude the model errors are generally below 30%,
165 which is deemed acceptable for analytical natural ventilation models (Zhai et al., 2016).
166 Notably, for buoyancy-driven cross ventilation, the error falls below 10%. Although these
167 errors are higher than for CFD modelling (less than 10% in neutral condition, i.e. no
168 temperature variability, van Hooff et al., 2017), the advantages of AFN lie in having a better
169 balance between accuracy and computational cost.

170 The SUEWS-EnergyPlus multiscale modelling scheme brings several advantages compared
171 to previous studies. First, both models have undergone rigorous evaluations, ensuring their
172 reliability and accuracy. Second, SUEWS has a modified MOST model (Harman and
173 Finnigan, 2007; Tang et al., 2021; Theeuwes et al., 2019) providing vertical profiles within
174 the roughness sublayer (RSL) of temperature, wind, and relative humidity for where the
175 buildings are located. Third, the scheme takes into account the impact of wind sheltering
176 effects by incorporating local wind profiles and correspondingly modified wind pressure
177 coefficient data (Xie et al., 2023). Fourth, the scheme considers the influence of inter-
178 building longwave radiative exchanges (Xie et al., 2022). With all combined (also shown in
179 Fig. 1), they create an effective, comprehensive multiscale modelling approach.

180 The objectives of this study are to: (1) improve EnergyPlus's ability to predict NVP in the
181 urban environment, (2) analyse impacts of urban climate on the NVP, and (3) investigate how
182 NVP changes with neighbourhood plan area fraction of buildings and climate.

Journal Pre-proof

Manuscript submitted to *Building and Environment*, revised July 2023

183 **Table 1:** Summary of studies on natural ventilation potential (NVP) by date. Weather data source: open - standard rural meteorological station; urban - on-site observation or
 184 CFD modelling. NVP Metric: NV-hours - natural ventilation hours; PDPH - pressure difference Pascal hours; NVCE – natural ventilation cooling effectiveness (Yoon et al.,
 185 2020), ratio of actual ventilation heat loss rate to required ventilation heat loss rate. NV criteria: T - air temperature, U -wind; RH - relative humidity. Method of NVP
 186 calculation: OutMet – outdoor meteorological data, BS - Building simulation, OuInMet - Outdoor/indoor data analysis.

City Location	NVP Method	Effective NV criteria				BS tool	Weather data	NVP Metric	Urban Met	Reference
		T	U	RH	Others					
Townsville, Australia	OutMet	√	√	√		-	Open	Number of occasions		(Aynsley, 1999)
Multiple China	BS	√	√			Own model	Open	PDPH		(Yang et al., 2005)
Athens, Greece	OutMet	√	√		Noise, pollution	-	Urban	No metrics - Method development	T, U	(Ghiaus et al., 2006)
Multiple China	BS	√	√			Own model	Open	NV-hours, PDPH		(Luo et al., 2007)
Basel, Switzerland	OuInMet	√	√		Noise, pollution	-	Urban	NV-hours	T, U	(Germano, 2007)
Multiple China	BS	√				Own model	Open	NV-hours		(Yao et al., 2009)
Multiple China	BS	√	√	√		Own model	Open	NV-hours		(Yin et al., 2010)
Vejle, Denmark	BS	√				EnergyPlus	Open	NV-hours		(Oropeza-Perez and Østergaard, 2013)
Multiple Europe	OuInMet	√	√			-	Open	NV-hours		(Faggianelli et al., 2014)
Multiple China	BS	√		√		DeST and CFD	Urban	Mean ventilation rate	T, RH	(Li and Li, 2015)
Multiple India	BS	√	√			TRNSYS	Open	PDPH		(Patil and Kaushik, 2015)
Multiple US	BS	√				EnergyPlus	Open	Target air change rate		(Hiyama and Glicksman, 2015)
State College, US	BS	√	√			IES-VE	Open	NV-hours		(Cheng et al., 2016)
Multiple Global	OutMet	√		√		-	Open	NV-hours		(Causone, 2016)
Multiple China	BS	√		√	Pollution	EnergyPlus	Open	NV-hours		(Tong et al., 2016)
Multiple US	OutMet	√	√	√		-	Urban	NV-hours	T, U, RH	(Tong et al., 2017)
Multiple Europe	BS	√			Pollution	EnergyPlus	Open	NV-hours		(Martins and Carrilho Da Graça, 2017)
Multiple Global	OutMet	√	√			-	Open	NV-hours		(Chen et al., 2017)
Multiple Australia	BS	√				TRNSYS	Open	NV-hours		(Tan and Deng, 2017)
Multiple Spain	BS	√		√		DesignBuilder	Open	NV-hours		(Pesic et al., 2018)
Multiple North America	BS	√				Own model + CFD	Open	NV-hours		(Cheng et al., 2018)
Boston, US	BS	√	√			Own model + CFD	Urban	NV-hours	T, U	(Wang and Malkawi, 2019)
Multiple China	BS	√				EnergyPlus	Open	NV-hours		(Chen et al., 2019)
Chongqing, China	BS	√			Pollution	EnergyPlus + CFD	Urban	NV-hours	T	(Costanzo et al., 2019)
Multiple US	BS	√	√			EnergyPlus	Open	NVE		(Yoon et al., 2020)

Manuscript submitted to *Building and Environment*, revised July 2023

Chambéry, France	BS	√	√		EnergyPlus	Open	NV-hours		(Sakiyama et al., 2021)
------------------	----	---	---	--	------------	------	----------	--	-------------------------

187

Journal Pre-proof

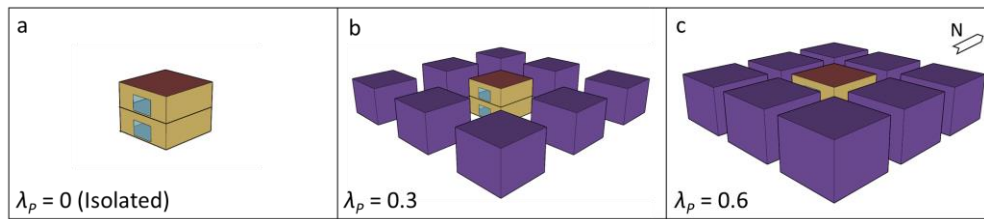
188 2. Methods

189 To study the impact of urban climate on building natural ventilation potential (NVP), we
190 couple the local-scale land surface model Surface Urban Energy and Water Balance Scheme
191 (SUEWS) v2021a (SuPy v2021.11.20) (Järvi et al., 2011; Sun et al., 2020; Sun and
192 Grimmond, 2019; Tang et al., 2021; Ward et al., 2016) and the building energy simulation
193 tool EnergyPlus v9.4 (U.S. Department of Energy, 2020a). Representative cities from five
194 different climate zones in China are selected to consider the climate variations.

195 2.1. Urban neighbourhood scale climate modelling

196 The urban surroundings could affect the natural ventilation of a building of interest (Fig. 2) in
197 multiple ways (Fig. 1) by directly impacting the driving potential of NV (buoyancy force and
198 wind-driven force). Specifically, the street geometry in a neighbourhood can result in a
199 decrease in wind speed, leading to a reduction in wind-driven natural ventilation rate. The
200 canopy layer urban heat island (UHI) can lead to smaller temperature differences between
201 indoor and outdoor air, which can reduce the buoyancy-driven natural ventilation rate. Here
202 we use an urban neighbourhood wind profile, which requires the use of modified wind
203 pressure coefficients based on differences between free-stream and urban neighbourhood
204 wind profiles in EnergyPlus (Xie et al., 2023).

205 SUEWS is used to model three idealised neighbourhoods (Fig. 2) that have different building
206 plan area densities but the same initial climate forcing data. The simulated energy and water
207 balance fluxes are used to diagnose local-scale meteorological variables for the three
208 neighbourhoods which are provided to EnergyPlus as the weather data for the building
209 energy simulations. SUEWS performance has been extensively evaluated and applied in
210 different climates globally (e.g. Table 3 of Lindberg et al. (2018); Table 1 of Sun and
211 Grimmond (2019)).



212

213 **Fig. 2.** Reference building (8 m × 8 m × 6.4 m) is simulated (EnergyPlus) after the weather data is simulated
 214 (SUEWS) for three neighbourhoods: (a) a rural (isolated), and two city neighbourhoods with building plan area
 215 fractions (λ_p) of (b) 0.3 and (c) 0.6.

216 SUEWS allow each neighbourhood to have varying amounts of seven land cover types:

217 paved, buildings, deciduous trees/shrubs, evergreen trees/shrubs, grass, bare soil and water.

218 This allows realistic intra-city land cover variations, between different cities. For simplicity,

219 here we assume neighbourhoods consist of buildings and grass (i.e., two typical but

220 contrasting surface types), so vegetation's influence (e.g., evapotranspiration) is considered

221 but more complicated impacts, such as trees/shrubs influence on wind (Kent et al., 2018) and

222 radiation (Morrison et al., 2018) are not included. Our three neighbourhoods are:

223 (a) *rural* (Fig. 2a): is a large area covered with 100% grass, hence the isolated building area

224 is negligible

225 (b) *medium density* (Fig. 2b): has buildings covering 30% of the area (plan area fraction $\lambda_p =$

226 0.3) and grass covering 70%

227 (c) *high density* (Fig. 2c): has $\lambda_p = 0.6$ and grass in the remaining 40% of the area

228 The SUEWS neighbourhood population density is consistent with the EnergyPlus building

229 occupancy (Section 2.2).

230 The Design Standard for Energy Efficiency of Public Buildings (MoHURD, 2015) classifies

231 China into five climate zones (Table 2) using typical average air temperatures in January and

232 July as the primary indicators. This classification aims to provide guidance on the design of

233 building envelope thermal characteristics for each specific climate zone and identifies the

234 major cities in the zone. Here we use the ERA5 (ECMWF Reanalysis version 5) (Hersbach et

235 al., 2020) meteorological data, which are available globally at a spatial resolution of 0.125°

236 and a temporal resolution of a hour. As natural ventilation cooling for buildings is
 237 particularly important during hot periods, we select 2018, the year with the warmest
 238 Northeast Asia summer (JJA) mean near-surface air temperature between 1979 and 2018 (K.
 239 Xu et al., 2019) for simulation. The three neighbourhoods are simulated in one city for each
 240 of the five climates (Table 2), assuming human activities do not vary between the regions.
 241 One ERA5 grid located in centre of the city is used. Note the ERA5 data do not account for
 242 urban land cover in the reanalysis but do assimilate meteorological data with cities (Tang et
 243 al., 2021). The vegetation cover assigned to the grid is representative of local conditions
 244 (Hersbach et al., 2020).

245 **Table 2.** Building thermal characteristics and specific city simulated in each climate zones in China. SHGC:
 246 solar heat gain coefficient. Modified from Tong et al. (2016).

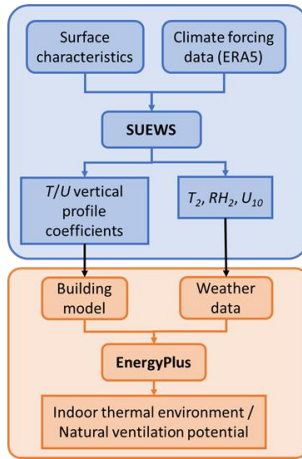
City	Climate zone	U-value ($\text{W m}^{-2} \text{K}^{-1}$)				SHGC
		Roof	External wall	Ground floor	Window	Window
Harbin	Very cold	0.25	0.35	0.25	1.76	0.68
Beijing	Cold	0.39	0.46	0.46	1.77	0.37
Shanghai	Cold winter hot summer	0.39	0.54	0.46	2.3	0.32
Kunming	Temperate	0.44	0.72	1.32	2.4	0.2
Guangzhou	Warm winter hot summer	0.44	0.72	1.32	2.4	0.2

247
 248 To drive SUEWS the meteorological data in the inertial sub layer or constant flux layer are
 249 needed. This layer is located above the roughness sub layer (RSL). Within the RSL individual
 250 roughness element influences the air flow, while above that the flow becomes blended and
 251 provides a neighbourhood or local scale response. The RSL extends from ground to a depth
 252 of approximate 2 to 5 times of mean roughness element height (i.e. buildings and trees) (Oke
 253 et al., 2017b), where the building are located and most human activities occur. Thus, SUEWS
 254 forcing height depends on both the building height (i.e. height above ground level) and the
 255 city altitude (height above sea level, see Fig. 1 in Tang et al. 2020). With a mean building
 256 height is 6.4 m (Fig. 2) the forcing height above ground level (agl) needs to be at least 12.8 to
 257 32 m agl. For example, central Kunming is located at an altitude of 1892 m above sea level
 258 (asl) (Liu et al., 2022), whereas the larger ERA5 grid-cell over central Kunming has an

259 altitude of 2000 m asl (or 108 m agl). Therefore for Kunming a forcing height of 108 m agl is
260 used. For climates with ERA5 height less than 32 m agl, The ERA5 data are adjusted to the
261 appropriate height using the environmental lapse rate following Tang et al.'s (2021) Appendix
262 B.

263 Building energy simulation of natural ventilation potential, requires wind speed U , air
264 temperature T and relative humidity RH in the RSL. Here we use the SUEWS-RSL module to
265 obtain the environmental variables. SUEWS-RSL calculates vertical profiles of these
266 variables with a RSL corrected MOST (Monin-Obukhov Similarity Theory) approach
267 (Harman and Finnigan, 2008, 2007; Theeuwes et al., 2019), while accounting for varying
268 atmospheric stability, roughness characteristics and turbulent heat fluxes (Tang et al., 2021;
269 Theeuwes et al., 2019). Evaluation of the SUEWS-RSL U and T profiles against observations
270 in three global cities, suggest an acceptable accuracy (Tang et al., 2021; Theeuwes et al.,
271 2019).

272 The SUEWS-RSL generated local weather data, includes T and RH at 2 m above ground (T_2
273 and RH_2), U at 10 m (U_{10}), and vertical profiles of T and U within the RSL (Fig. 3). The
274 supplied T_2 , RH_2 and U_{10} as well as other climate data (e.g., incoming solar radiation from
275 ERA5) are formatted as a EnergyPlus weather file (.epw). The SUEWS-RSL wind profile is
276 passed to EnergyPlus via input files (.idf) by replacing the power law coefficients with values
277 derived from the SUEWS-RSL data.



278

279 **Fig. 3.** Overview of the SUEWS-EnergyPlus workflow integration (Tang et al., 2021).

280 In EnergyPlus solar shading from adjacent buildings (purple, Fig. 2) are simulated as
 281 ‘shading objects’. The longwave radiative exchanges between the reference building and
 282 adjacent buildings are calculated with an iterative approach (Xie et al., 2022). Impacts of
 283 other urban factors like the heat storage and the anthropogenic heat are simulated with
 284 SUEWS and accounted for in the outdoor air temperature (Fig. 1, Fig. 3).

285 2.2. Building characteristics

286 To compare the NVP, a two-storey building model (Fig. 2a) based on ASHRAE Case 600
 287 (ANSI/ASHRAE, 2011) is developed in EnergyPlus. The 8 m wide × 8 m long × 6.4 m tall,
 288 building has no interior partitions. There are two windows on each floor, one on the south-
 289 facing and one on the north facing-wall to provide natural ventilation. All four windows are 2
 290 m × 3 m. A simplified residential occupancy (2 people on each floor, 125.6 W person⁻¹,
 291 occupied all-day) and internal heat gain (lighting: 6 W m⁻², equipment: 4.3 W m⁻²) are
 292 assumed (Xiong et al., 2019). The simulated reference building is assigned the Design
 293 Standard for Energy Efficiency of Public Buildings (MoHURD, 2015) thermal characteristics
 294 appropriate for each climate zone (Table 2).

295 For the NVP analysis, we consider both cross and single-sided ventilation (only south-facing
 296 windows open). All windows are assumed to have 15% openable area and discharge

297 coefficient (C_d) of 0.61. For the cooling energy savings calculation, an ideal load system is
298 assumed with a heating setpoint of 18 °C and cooling setpoint of 26 °C based on the
299 recommendation of the Code for Thermal Design of Civil Building (MoHURD, 2016).

300 2.3. *Natural ventilation models*

301 To simulate the cross ventilation the Airflow Network (AFN) model within EnergyPlus is
302 used (U.S. Department of Energy, 2020b). The AFN has been evaluated and widely used for
303 natural ventilation calculations (Johnson et al., 2012). The AFN airflow rate is calculated
304 using the pressure difference across openings, with the standard orifice flow equation. The
305 wind-driven ventilation rate V_w is (Awbi, 2003):

$$306 \quad V_w = C_d A \sqrt{\frac{2\Delta P_w}{\rho_0}} \quad (1)$$

307 where C_d is the discharge coefficient of opening, A is the effective opening area (m^2), ρ_0 is the
308 outdoor air density (kg m^{-3}) and ΔP_w is the wind pressure difference across opening (Pa). The
309 wind pressure at the opening height is (Awbi, 2003):

$$310 \quad P_w = 0.5\rho_0 C_p U_{free}^2 \quad (2)$$

311 where C_p is the surface-averaged wind pressure coefficient, and U_{free} is the upstream
312 undisturbed flow at the opening height.

313 As C_p values are influenced by the building geometry, surrounding conditions and wind
314 profile and direction (Grosso, 1992), it is important to use the appropriate C_p values as it
315 impacts the accuracy of the building natural ventilation simulation in an urban environment.

316 In this study, TPU *Aerodynamic Database of Non-isolated Low-Rise Buildings* (TPU, 2007)

317 C_p data from wind-tunnel experiments for buildings with different geometries and

318 surrounding conditions are used. As the TPU C_p database is for free-stream wind measured in

319 wind tunnel experiments, we modified these using the SUEWS-RSL wind speeds and profile
320 as shown in Xie et al. (2023).

321 Although it is widely accepted that cross ventilation usually achieves much larger ventilation
322 rate, it is less practical than single-sided ventilation for urban buildings where isolated rooms
323 are common (Zhong et al., 2022). The single-sided ventilation model, based on the mixing
324 layer theory (Warren, 1977; Warren and Parkins, 1984), is used. This has been evaluated in
325 wind-tunnel and full scale experiments (Gough et al., 2020; Yamanaka et al., 2006). The
326 wind-driven ventilation rate (V_w , $\text{m}^3 \text{s}^{-1}$) is calculated with:

$$327 \quad V_w = 0.1AU \quad (3)$$

328 From Bernoulli principles, the buoyancy-driven ventilation rate (V_b) is calculated with:

$$329 \quad V_b = \frac{c_d A}{3} \sqrt{gh_{\text{opening}} \frac{\Delta T}{T}} \quad (4)$$

330 where g is the gravitational acceleration, h_{opening} the height of the opening, ΔT air temperature
331 difference across the opening. The total ventilation rate (V_t) is the quadrature sum of the wind
332 and stack air flow components (U.S. Department of Energy, 2020c):

$$333 \quad V_t = \sqrt{V_w^2 + V_b^2} \quad (5)$$

334 2.4. Analysis metrics

335 In this study, the natural ventilation hours (NV-hour) and the cumulative air change rate
336 (ACH-hour) are used to quantify the natural ventilation potential (NVP).

337 The NV-hour, the most common NVP metric (Table 1), is the number of hours per year when
338 natural ventilation can fulfil both the air quality and thermal comfort requirements (Luo et al.,
339 2007; Yin et al., 2010). ASHRAE Standard 62.1 (ANSI/ASHRAE, 2013) defines the required
340 minimum outdoor airflow rate (V_R) for a residential space as a function of the number of
341 people occupying (N_p) the floor area (A_f , units: m^2) as:

$$342 \quad V_R = 0.0025N_p + 0.0003A_f \quad (6)$$

343 In this study, as each floor has $N_p = 2$ and $A_f = 64 \text{ m}^2$, $V_R = 0.0242 \text{ m}^3 \text{ s}^{-1}$ ($\approx 0.425 \text{ ACH}$).

344 For free-running building thermal comfort assessment, we use the Chinese adaptive thermal
 345 comfort models provided in the *Evaluation Standard for Indoor Thermal Environment in*
 346 *Civil Buildings* (MoHURD, 2012) for 75% satisfaction (or Category II). These specify an
 347 upper (T_{UL}) and lower indoor operative temperature limit (T_{LL}) by zone, with the northern
 348 (very cold, cold, Table 2):

$$349 \quad \begin{cases} T_{UL,N} = 0.73T_{rm} + 15.28 & (18^\circ\text{C} \leq T_{UL,N} \leq 30^\circ\text{C}) \\ T_{LL,N} = 0.91T_{rm} - 0.48 & (16^\circ\text{C} \leq T_{LL,N} \leq 28^\circ\text{C}) \end{cases} \quad (7)$$

350 and southern zones (cold winter hot summer, temperate, warm winter hot summer, Table 2):

$$351 \quad \begin{cases} T_{UL,S} = 0.73T_{rm} + 12.72 & (18^\circ\text{C} \leq T_{UL,S} \leq 30^\circ\text{C}) \\ T_{LL,S} = 0.91T_{rm} - 3.69 & (16^\circ\text{C} \leq T_{LL,S} \leq 28^\circ\text{C}) \end{cases} \quad (8)$$

352 This uses a seven day ($n = 7$) running mean of the outdoor air temperature (T_{rm}):

$$353 \quad T_{rm} = (1 - k)(T_{od-1} + \alpha T_{od-2} + \alpha^2 T_{od-3} \cdots + \alpha^6 T_{od-7}) \quad (9)$$

354 where k is a constant between 0 and 1, with 0.8 as recommendation (Nicol and Humphreys,
 355 2010), and T_{od-n} is the daily mean outdoor air temperature for n days ago ($^\circ\text{C}$).

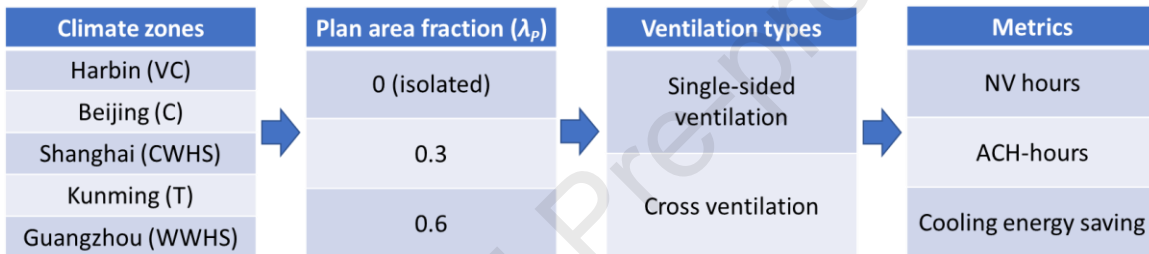
356 As higher ventilation rates may prevent sick building syndrome symptoms and reduce
 357 potential airborne infection risk (Sundell et al., 2011), we also determine the ACH-hour, or
 358 cumulative air change rate during the NV-hour period. This is similar to pressure difference
 359 Pascal hours (PDPH) (Yang et al., 2005). Although both aim to quantify availability of
 360 natural driving forces, ACH-hour is more directly linked to amount of ventilation.

361 Cooling energy saving (Q_{saving}) is also determined (Tong et al., 2016):

$$362 \quad Q_{saving} = Q_{window_closed} - Q_{window_open} \quad (10)$$

363 The is the difference in energy demand between a fully air-conditioned building (i.e.
 364 windows always closed, Q_{window_closed}) and a hybrid-controlled building with windows open
 365 (Q_{window_open}) when the indoor air temperature can vary between the heating and cooling set
 366 points (18 to 26 °C) while the air conditioning system is turned off. The air-conditioning
 367 system setting are given in section 2.1.

368 In summary (Fig. 4), three metrics are determined from analysis of simulations for five
 369 climates and for three neighbourhoods with different plan area fractions (λ_P) and two
 370 ventilation types. Thus, a total of ($5 \times 3 \times 2 =$) 30 cases are simulated.



371
 372 **Fig. 4.** Variables and metrics analysed in this study. See Fig. 2 and Table 2 for more details.

373

374 We use mean the bias error (MBE) to assess the difference between SUEWS-RSL and
 375 modified EnergyPlus wind profiles (Eq. 12, Table 3 coefficients):

$$376 \quad MBE = \frac{1}{N} \sum_{i=1}^N (y_i - x_i) \quad (11)$$

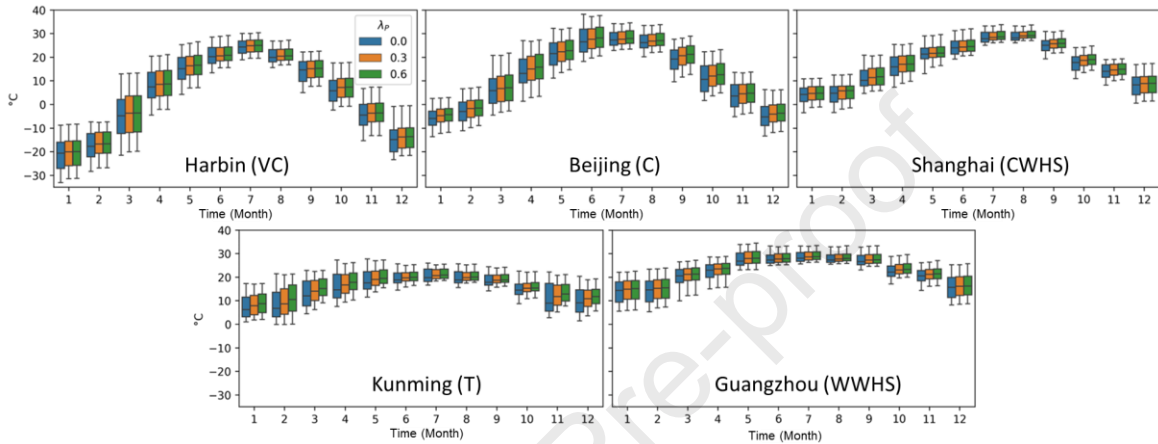
377 where y_i and x_j are EnergyPlus and SUEWS-RSL wind speeds at each timestep, and N is the
 378 number of values analysed (i.e. a year with hourly timestep, $N = 8760$).

379 3. Results

380 3.1. Outdoor climate

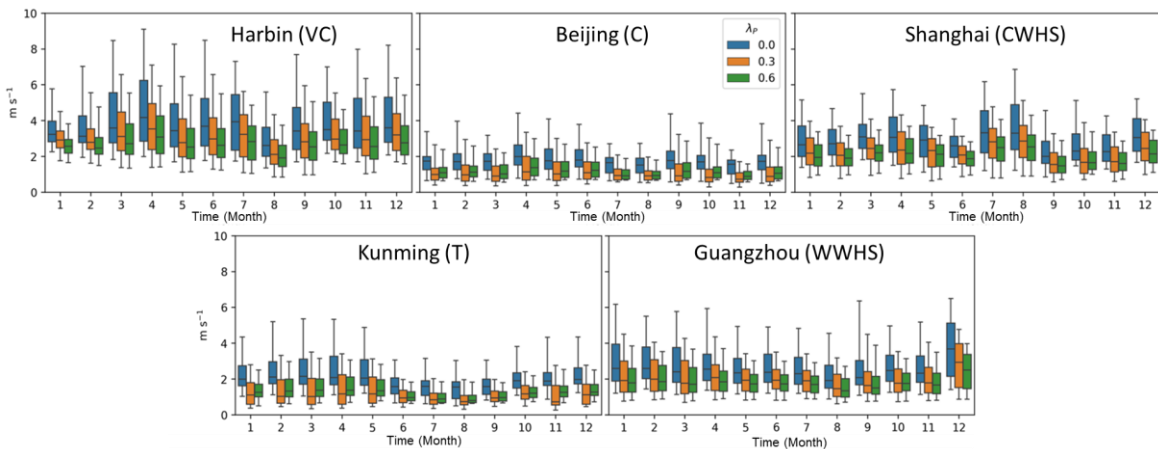
381 First, we assess differences in modelled local environmental variables for the neighbourhoods
 382 with different building plan area fractions (λ_P) and in different climate zones (Fig. 4).

383 Modelled outdoor air temperature at 2 m (T_2) in denser neighbourhoods (larger λ_P , green Fig.
 384 5) have warmer monthly values and greater variation than at the rural site in all five climates
 385 (blue, Fig. 5). Annual mean differences in T_2 between cases with λ_P of 0.6 and 0 vary
 386 between 0.8 °C in Guangzhou and 1.6 °C in Kunming. This difference is indicative of the
 387 canopy layer urban heat island effect.



388
 389 **Fig. 5.** Monthly distribution (hourly) of modelled outdoor air temperature at 2 m agl for three plan area fraction
 390 of buildings (λ_P , Fig. 2; colours) and five climates (Table 2), with interquartile range (box), median (horizontal
 391 line) and 5th and 95th percentiles (whiskers).

392 Whereas the monthly variation of SUEWS-RWL modelled wind speed at 10 m (U_{10})
 393 decrease as λ_P increases (Fig. 6). The annual mean differences ($\Delta\lambda_P$ 0.6 \rightarrow 0) are smallest in
 394 Beijing (0.6 m s⁻¹) to and larges in Harbin (1.1 m s⁻¹). These results are qualitatively similar
 395 to previous CFD studies considering outdoor velocity and λ_P (e.g. Mei et al. (2017)).

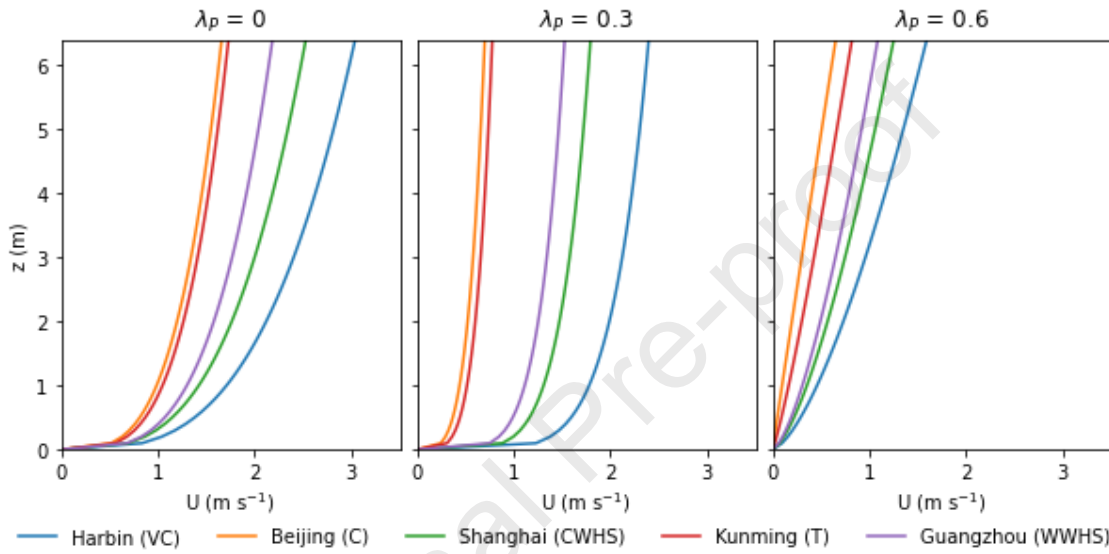


396
 397 **Fig. 6.** As Fig. 5, but wind speed at 10 m agl.

398 Vertical wind profiles (Fig. 7) derived SUEWS-RSL are used to calculate the EnergyPlus
 399 power-law parameters (δ , α , Table 3)(ASHRAE, 2005):

$$400 \quad U_z = U_{10} \left(\frac{\delta_{ref}}{10} \right)^{\alpha_{ref}} \left(\frac{z}{\delta} \right)^\alpha \quad (12)$$

401 where the meteorological station boundary layer depth (δ_{ref}) and exponent (α_{ref}) are obtained
 402 as the default settings in EnergyPlus for open terrain (U.S. Department of Energy, 2020d).



403
 404 **Fig. 7.** Vertical wind profiles for three different λ_p and five climates (colour) calculated with annual median 10
 405 m wind speeds and coefficients (Table 3) derived from the SUEWS-RSL results (EP_{RSL}) within the canopy layer
 406 (building height= 6.4 m).
 407

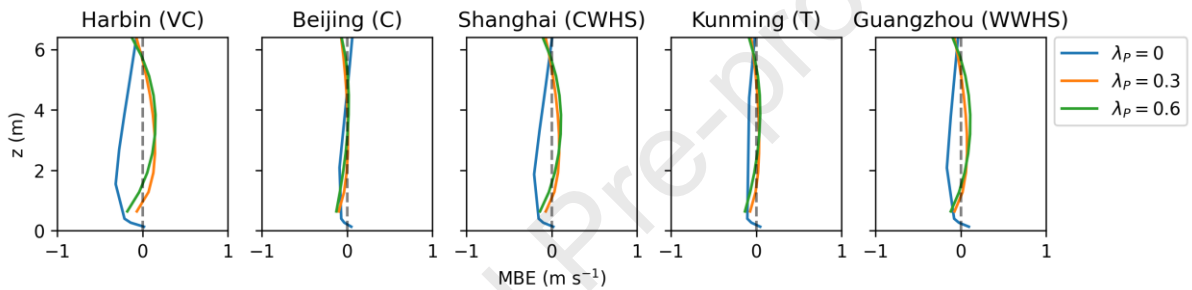
408 **Table 3:** Wind power law (Eq. 12) coefficients derived from SUEWS-RSL model output for each climate and
 409 neighbourhood.

λ_p	Exponent α					Boundary layer depth δ (m)				
	Harbin (VC)	Beijing (C)	Shanghai (CWHS)	Kunming (T)	Guangzhou (WWHS)	Harbin (VC)	Beijing (C)	Shanghai (CWHS)	Kunming (T)	Guangzhou (WWHS)
0	0.31	0.28	0.31	0.27	0.28	40.41	37.88	37.34	46.62	46.93
0.3	0.16	0.25	0.17	0.22	0.17	380.44	125.28	322.01	149.76	320.19
0.6	0.67	1.02	0.68	0.86	0.68	25.96	16.16	25.11	16.65	24.87

410

411 To assess the mean bias error (MBE) for the EnergyPlus wind profiles when using the Table
 412 3 coefficients (hereafter EP-RSL profiles), we use the original SUEWS-RSL vertical wind
 413 profiles data which varying because of the different forcing heights; (5 to 8 vertical levels for
 414 $\lambda_p = 0$; 9 levels at $\lambda_p = 0.3$ and 0.6) as the baseline (Fig. 8). As the SUEWS-RSL wind profile
 415 does not assume a power law and varies with stability (Tang et al., 2021; Theeuwes et al.,

416 2019), biases still exist in EP-RSL profiles. The biases are larger for climates with stronger
 417 wind speeds (e.g. Harbin). When $\lambda_P = 0$, the EP-RSL profiles underpredicts the median wind
 418 speeds by up to 0.35 m s^{-1} , especially around 2 m above ground level. For $\lambda_P = 0.3$ the EP-
 419 RSL $\text{MBE}_{\text{median}}$ are smaller ($\leq 0.2 \text{ m s}^{-1}$), as are $\lambda_P = 0.6$ cases. As the $\text{MBE}_{\text{median}}$ become
 420 better (smaller) with height within the canopy layer ($> 3.2 \text{ m}$), we focus analysis on the upper
 421 floor natural ventilation potential and energy saving. Future work could directly use the RSL
 422 wind profile within EnergyPlus after rewriting the appropriate code. This is beyond the scope
 423 of this study.



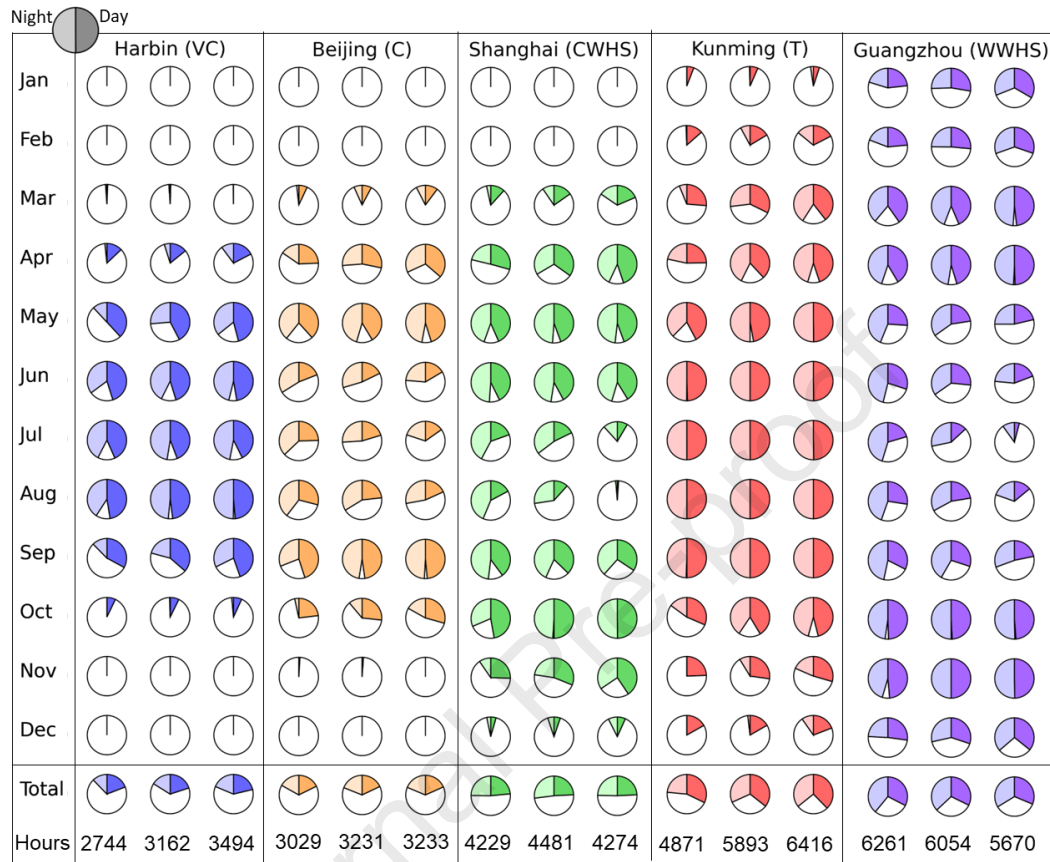
424 **Fig. 8.** Annual mean bias error (MBE) for wind speed calculated at hourly timestep but vertical resolution (Δz)
 425 that varies (from 0.13 m with varying Δz for $\lambda_P = 0$; from 0.64 m with $\Delta z = 0.64 \text{ m}$ for $\lambda_P = 0.3$ and 0.6) to 6 m
 426 above ground level; where SUEWS-RSL (x , Eq. 11) and EP-RSL wind profiles (y , Eq. 11; using Eq. 12, and
 427 Table 3 coefficients) for three λ_P (colour) and five climates.
 428
 429

430 3.2. Natural ventilation potential (NVP)

431 3.2.1. Natural ventilation hours (NV-hour) of cross ventilation

432 Cross ventilation monthly percentage of NV-hours across the five climates (Table 2) and
 433 three λ_P classes (Fig. 2) are generally larger for upper floor room (Fig. 9). With windows
 434 always opened, the minimum ventilation rate requirement of 0.425 air change per hour
 435 (ACH) (section 2.4) can be fulfilled during most of the year (Fig. 9). Although the Beijing
 436 neighbourhood with $\lambda_P = 0.6$ has the lowest wind speeds, there are only 23 hours within the
 437 year that do not meet the ventilation rate criteria. Thus, differences in NV-hours are mostly
 438 influenced by the thermal comfort criteria. As a result, warm climates (Guangzhou, Kunming,

439 Shanghai) have more annual total NV-hours than cold climates (Harbin, Beijing), since there
 440 is very limited NV potential for cold climates in winter (Fig. 9).



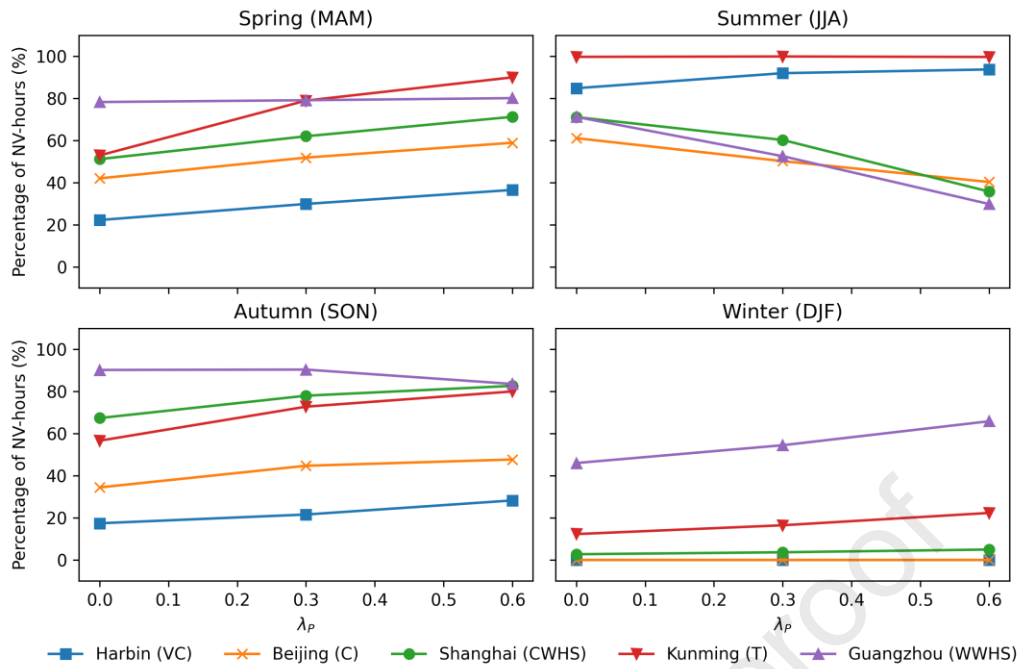
441
 442 **Fig. 9.** Upper floor cross ventilation as percentages of NV-hours (relative to total hours in the period for five
 443 climates (columns), three neighbourhoods (λ_P colours, blue: 0; green: 0.3; red: 0.6) and different time intervals
 444 (rows: monthly and annual, time of day (pie chart half): right daytime (7:00 to 19:00), left night-time (19:00 to
 445 7:00)).

446 Influences of λ_P on NV-hours vary across climates (Fig. 9). In terms of the annual total, the
 447 building in the $\lambda_P = 0$ rural neighbourhood has the most annual NV-hours in hot climates like
 448 Guangzhou. While for low-medium density $\lambda_P = 0.3$, warm winter hot summer climates like
 449 Shanghai have the most annual NV-hours. Dense urban neighbourhoods ($\lambda_P = 0.6$) have the
 450 most annual NV-hours in cold northern zones including Harbin and Beijing, and the mild
 451 climates like Kunming. This can be explained by the air temperature distribution (Fig. 6) as
 452 dense neighbourhoods ($\lambda_P = 0.6$) tend to have higher outdoor temperatures (in their regional
 453 climate), which is beneficial in cool climates for thermal comfort, and vice versa. The annual
 454 differences in NV-hours between $\lambda_P = 0$ and $\lambda_P = 0.6$ is largest in Kunming (1545) which is

455 more than twice the difference to the next largest (Harbin, 753). The others are smaller again
456 Guangzhou (587), Shanghai (254), and smallest in Beijing (201).

457 The λ_P has a greater impact on nocturnal NV-hours than daytime (Fig. 9), linked to the larger
458 night-time temperature differences (Fig. 5). During cool months there are larger proportion of
459 daytime NV-hours, but the nocturnal NV-hours increases with λ_P to a greater extent (e.g.
460 nocturnal NV-hours increase by 33.9% while daytime increase by 13.2% from $\lambda_P = 0$ to 0.6
461 during March in Kunming). While in warm months, nocturnal NV-hours are reduced more
462 with the increase of λ_P (e.g. nocturnal NV-hours decrease by 35.3% while daytime increase
463 by 16.3% from $\lambda_P = 0$ to 0.6 during July in Guangzhou).

464 Generally, the dependence of NV-hours change with λ_P is highly related to climate and
465 seasons (Fig. 10). In summer, very cold climates (e.g. Harbin) have an increase in NV-hours
466 with λ_P (10% $\lambda_P = 0.6$ c.f. $\lambda_P = 0$), while the opposite occurs in hot summer climates regions
467 (-43% $\lambda_P = 0.6$ c.f. $\lambda_P = 0$ in Guangzhou). Whereas in the temperate climate (e.g. Kunming)
468 λ_P has negligible impact on NV-hours, as temperatures have both small variations and are
469 usually pleasant for indoor thermal comfort (Fig. 9). In winter, NV-hours increase with λ_P in
470 all regions due to cooler outdoor air temperatures, but the increase is small in regions with
471 cold winter and little natural ventilation potential including Harbin, Beijing and Shanghai.
472 During the spring/autumn transition seasons, the NV-hours tend to increase with λ_P in most
473 climates associated with the relatively mild outdoor climate except Guangzhou, where the
474 warm climate causes the indoor air temperature to exceed the upper limit of thermal comfort
475 in late spring (May) and early autumn (September) (Fig. 9).



476
477
478
479

Fig. 10. Seasonal upper floor with cross ventilation (**percentage of NV hours**) in five climates (colour) for three λ_P (marker).

480

3.2.2. ACH-hours of cross ventilation

481

The air exchange rates can enhance the NV benefits for air quality purposes. The annual

482

variability in ACH (hourly) during NV period (Fig. 11) is the largest when buildings are sited

483

in open areas ($\lambda_P = 0$) because of the higher variability of wind speed (Fig. 6 and 8), with

484

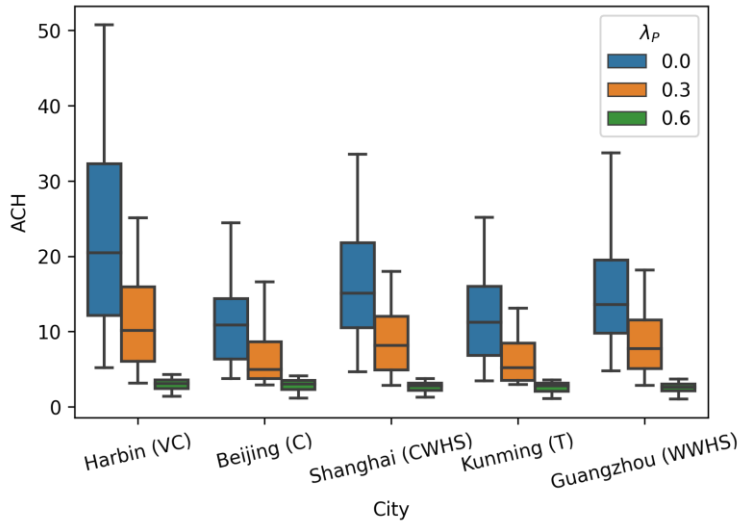
median ACH between 10.8 (Beijing) and 20 (Harbin). As λ_P increases the median ACHs

485

become smaller ($\lambda_P = 0.3$: 4.9 (Beijing) and 10.1 (Harbin); $\lambda_P = 0.6$: 2.6 (Beijing) and 3.0

486

(Harbin)).



487

488 **Fig. 11.** Annual variability in air changes per hour (ACH) when the upper floor cross ventilation (NV-hour >0)
 489 through the year for five climates and three λ_P (colours) with interquartile range (box), median (horizontal line)
 490 and 5th and 95th percentiles (whiskers).

491 The annual cumulative ACH-hours differs from NV-hours with λ_P variations. As ACH-hours

492 largely depend on wind speeds and ACH-hours decrease with λ_P in all climates (Fig. 12), the

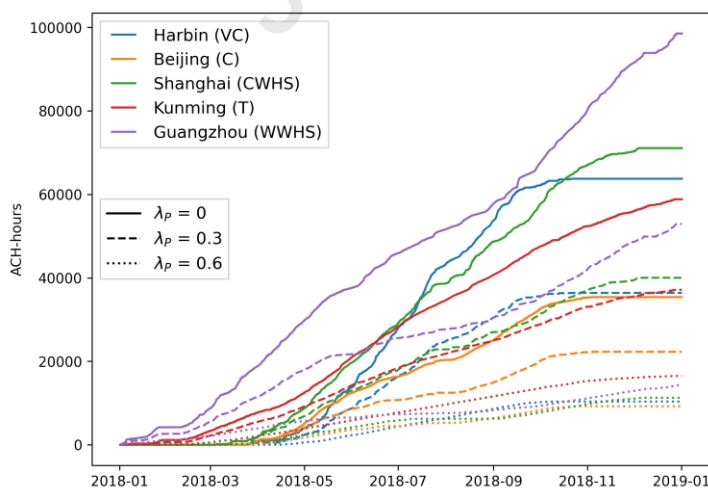
493 inter-climate variations are smaller (Fig. 12). Given the large number of annual NV-hours,

494 buildings in areas with a λ_P of 0 and 0.3 in Guangzhou and $\lambda_P = 0.6$ in Kunming have the

495 most ACH-hours (cf. to buildings in the same λ_P neighbourhoods but different climates).

496 While Beijing has the least annual ACH-hours for all λ_P due to low both ventilation rate and

497 NV-hours.

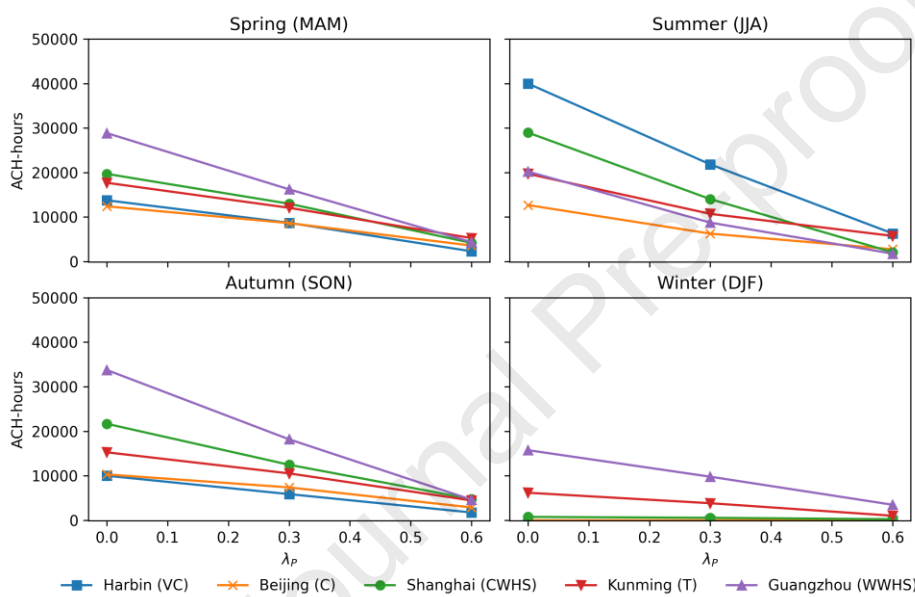


498

499 **Fig. 12.** Annual cumulative ACH-hours of the upper floor with cross ventilation across different climates
 500 (colour) and λ_P (line style).

501

502 The seasonal variations in ACH-hours are also influenced by both NV-hours and ventilation
 503 rates (Fig. 13). In transition seasons (spring/autumn), Guangzhou's climate has the largest
 504 ventilation potential in both ACH-hours and NV-hours (Fig. 10) benefiting from appropriate
 505 air temperatures and wind speeds, while Kunming's ranking drops due to the low ventilation
 506 rates. In summer, high wind speeds and mild summer temperatures make Harbin the climate
 507 with the most ACH-hours. The ranking of ACH-hours in winter remains consistent with the
 508 NV-hours.



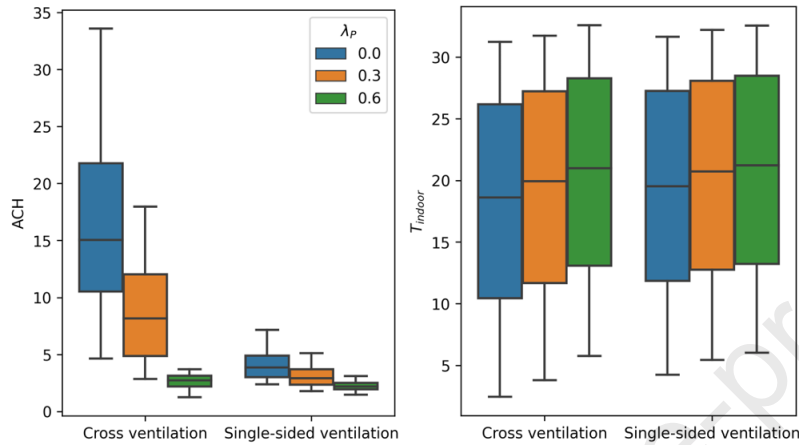
509

510 **Fig. 13.** Seasonal upper floor **ACH-hours** with cross ventilation in five climates (colour) for three λ_p (marker).

511 3.2.3. Single sided ventilation

512 To assess NVP differences between cross ventilation and single-sided ventilation we focus on
 513 Shanghai as similar conclusions are drawn for the other cities. Ventilation rates are largely
 514 less for single-sided ventilation (cf. cross ventilation) (Fig. 14) with annual median ACH
 515 reducing from 15.1/8.2/2.7 (cross ventilation) to 3.9/2.9/2.1 (single-sided ventilation) across
 516 the three plan area densities ($\lambda_p = 0/0.3/0.6$). This also implies that the single-sided
 517 ventilation is as effective as cross ventilation for buildings located in dense urban areas.
 518 Although the ventilation rates are reduced, the annual minimum ventilation rate for the

519 single-sided ventilation building even for $\lambda_P = 0.6$ (0.59 ACH), still meets the requirement of
 520 indoor air quality. Therefore, in Shanghai the natural ventilation potential is mainly
 521 influenced by thermal comfort criteria only. However, we do not consider the impact of
 522 outdoor air pollution (i.e., assuming outdoor air is unpolluted).



523 **Fig. 14.** Annual variability in upper floor air changes per hour (ACH) (left) and indoor air temperature (right)
 524 but for Shanghai for two ventilation modes.
 525

526 The reduced ventilation cooling potential with single-sided ventilation causes median indoor
 527 air temperature to increase by 0.9/0.8/0.2 °C for $\lambda_P = 0/0.3/0.6$ (Fig. 14). The seasonal
 528 percentage of NV-hours with single-sided ventilation therefore increases by up to 10.6 % (λ_P
 529 = 0) during spring and autumn, but decreases by up to 14.7 % ($\lambda_P = 0.3$) in summer (cf. cross
 530 ventilation) (Fig. 15). The ACH-hours are higher with cross ventilation in all conditions due
 531 to the higher ventilation rate, and differences between ventilation modes decreases as λ_P
 532 increases (Fig. 16).

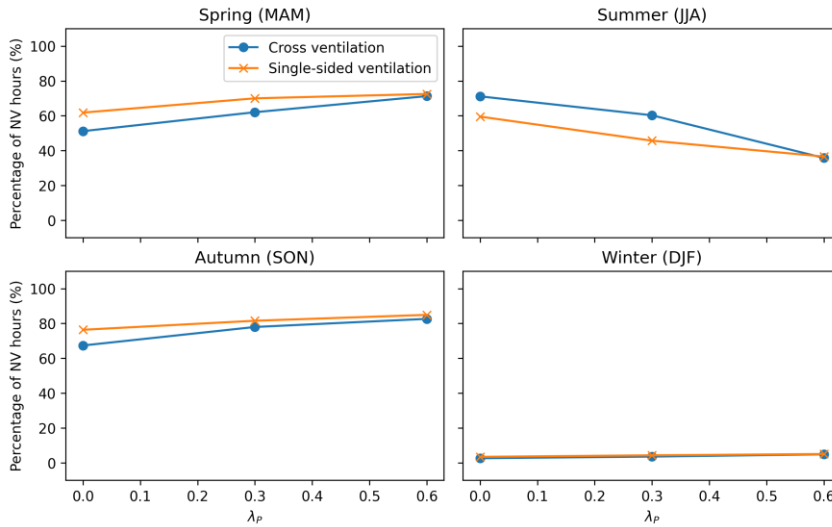
533
534
535

Fig. 15. Seasonal upper floor with cross ventilation (percentage of NV hours) in Shanghai for two ventilation modes.

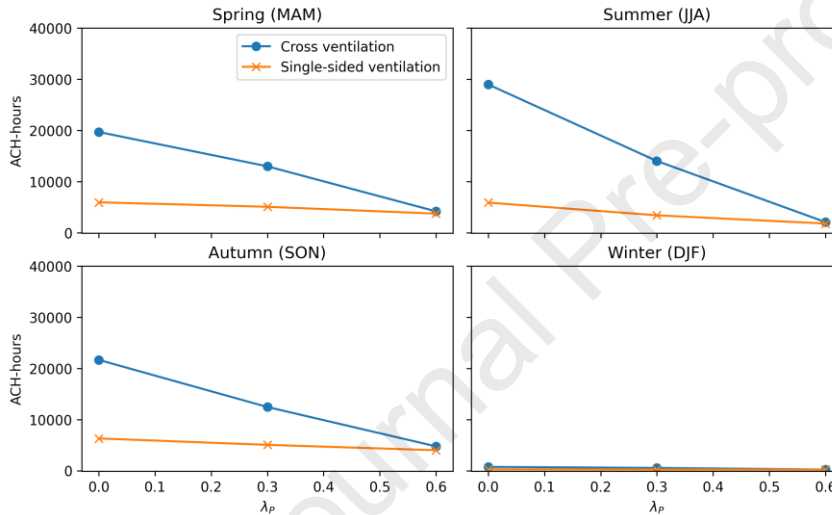
536
537

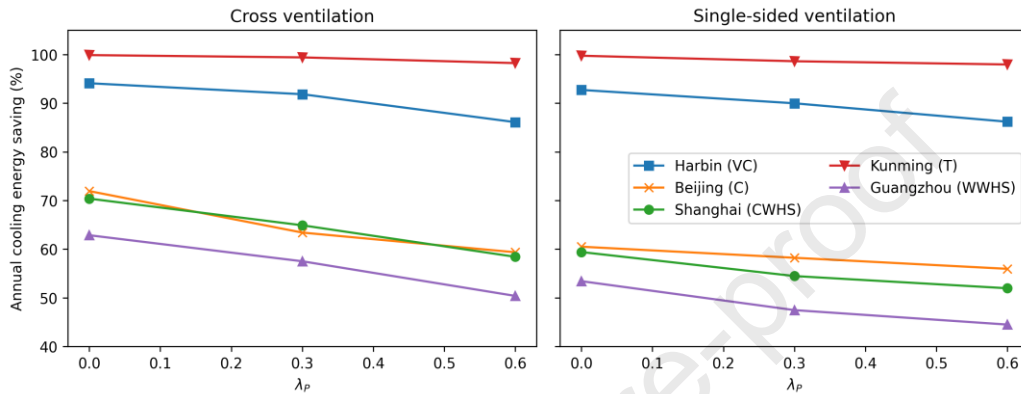
Fig. 16. Seasonal upper floor ACH-hours with cross ventilation in Shanghai for two ventilation modes.

538 Generally, the single-sided ventilation leads to lower ventilation rates across λ_p , and reduce
539 the natural ventilation potential in magnitude. The changing pattern of NVP with λ_p is similar
540 to cross ventilation,

541 3.3. Cooling energy saving

542 The cooling energy saving is calculated as the difference in cooling energy demand between
543 a building with air-conditioning only and hybrid ventilation (air-conditioning plus natural
544 ventilation). Therefore, the cooling energy saving amount is linked with the effectiveness of
545 natural ventilation cooling (Eq. 10). Cooling energy saving is expected to be larger for
546 climates and neighbourhoods with lower outdoor air temperatures and higher wind speeds.

547 Hence, in all climates the cooling energy saving decreases as λ_P increases (Fig. 17). For cross
 548 ventilation, such decreases are smallest in Kunming, as the climate is mild and temperature
 549 variation is small, making natural ventilation cooling available most of the time. For the other
 550 climates the cooling energy saving between building densities (λ_P) are similar (Harbin: 8% to
 551 Beijing: 12.5%).



552
 553 **Fig. 17.** Seasonal upper floor with cross ventilation annual cooling energy saving (Eq. 10, percentages) in five
 554 climates (colour) and two ventilation modes.

555 Our results differ slightly from Ramponi et al. (2014)'s nocturnal ventilation cooling energy
 556 saving study of three European cities. They suggest inter- λ_P differences are largely influenced
 557 by the climate, with natural ventilation cooling energy saving dropping by 20% in cool but
 558 windy Amsterdam, while in warmer less windy Milan (2 %) and Rome (13 %) reductions are
 559 less. Differences may arise from their different approach, as their outdoor air temperatures
 560 and wind speeds are independent of λ_P (only C_p values changed), and longwave radiative
 561 exchanges are not considered. The last may be critical as increased λ_P can result in more
 562 trapped longwave radiation, increasing building cooling demand (Xie et al. 2022). Our work
 563 highlights the importance of a holistic consideration of the complex interaction between
 564 urban climate and building performance.

565 Compared to cross ventilation, single-sided ventilation has less cooling energy savings due to
 566 lower wind speeds. The trends across climates are similar, despite slightly smaller inter- λ_P
 567 variations (6.5% to 8.1% excluding Kunming).

568 4. Discussion and conclusions

569 Although NVP across China's climate zones has been assessed previously, given the large
570 dependence on research approach, climate data and building model used, the results vary
571 (Luo et al., 2007; Tong et al., 2016; Yang et al., 2005; Yao et al., 2009). However, the urban
572 factors influencing buildings in an urban environment are often not fully considered.

573 In this study, we propose a multi-scale modelling scheme that combines the urban land
574 surface model SUEWS and building energy simulation tool EnergyPlus to assess the natural
575 ventilation potential (NVP) of buildings in different Chinese climate zones and
576 neighbourhoods with different building plan area fractions (λ_P). Unlike traditional approaches
577 that treat buildings as being isolated and use rural weather data, our approach considers
578 multiple urban factors, including the influence of the urban neighbourhood morphology on
579 canopy air temperature, wind sheltering effects, overshadowing, and longwave radiative
580 exchanges. Compared to computationally intensive methods like CFD, our approach offers
581 practical advantages in terms of simplicity and computational cost. The SUEWS model only
582 requires some commonly available surface characteristics and meteorological forcing data. A
583 year long run for one neighbourhood normally takes around 1 minute (PC) which is around
584 10^6 times less than CFD-based approaches (e.g. 3-day run taking 168 hours on PC by Yang
585 et al. (2012)). Therefore, our approach can be applied for quick estimates of natural
586 ventilation potential and cooling energy saving in larger scales (e.g. intra-city
587 neighbourhoods) for longer time periods. Also, the outputs by SUEWS can be used as
588 boundary conditions for CFD simulation.

589 We find that climate, plan area fraction and season combine to impact the NVP. Our findings
590 improve current understanding and design of NVP of urban buildings from a local climate
591 perspective. Local climate in denser areas have been shown to reduce NVP due to warmer
592 outdoor air temperatures on several summer days in Basel (cf. the rural area) (Germano,

2007) and reduced wind speeds from increasing λ_P ($0 \rightarrow 0.2$) reducing annual mean wind-driven ventilation rate by up to 35% (Li and Li, 2015). Given these studies, our findings further suggest that under different conditions, increasing the λ_P can either increase or decrease the NVP. For example, in summer, when the λ_P increases from 0 to 0.6, NV-hours increase by around 10% in Harbin (very cold) but decrease by around 43% in Guangzhou (warm winter hot summer). However, a critical disadvantage of urban areas is the low wind speeds, which leads to lower ventilation rates (e.g. Harbin: annual median ventilation rate reduced by 50% at $\lambda_P = 0.3$ and 85% at $\lambda_P = 0.6$). Hence, we should consider both NV-hours and ACH-hours. It is also found that single-sided ventilation can be as effective as cross ventilation in dense urban areas due to the low wind speed regardless of the metric used.

In this study we consider three metrics: NV-hour, ACH-hour, and cooling energy saving. The NV-hour, commonly used to measure NVP, gives the duration (in hours) suitable for natural ventilation. This metric is appropriate when considering general buildings without specific ventilation requirements. Limitation of the NV-hour metric includes its primarily reliance on thermal comfort based on indoor temperature and considers only a minimum ventilation rate limit, disregarding variations in ventilation rates determined by wind speed. To address this limitation, we introduce the ACH-hour, which incorporates ventilation rates based on the NV-hour and accounts for the influence of wind speed. The ACH-hour can offset the impact of temperature by considering high wind speeds and larger ventilation rates. For instance, even though Kunming has a milder climate and more NV-hours, the annual ACH-hours in Harbin are greater at $\lambda_P = 0$. Additionally, ACH-hours consistently decrease as λ_P increases. Therefore, the ACH-hour is more appropriate when ventilation rate is a critical factor. Whilst, the cooling energy saving metric (units: %) is influenced by both NVP and the original cooling demand. Climates with cooler summers, such as Harbin and Kunming, have higher percentages of cooling energy saving. This metric is particularly relevant for buildings with

618 mixed-mode ventilation systems. Hence, these metrics are useful for different applications
619 when considering the building and climate being evaluated.

620 Our approach offers a quick assessment of NVP for buildings in the urban environment. We
621 model idealised neighbourhoods with simplified building models based on relevant
622 observations and standards, although we acknowledge that real cities are more complex.
623 Natural ventilation depends on factors like building and room geometry. In this study we use
624 a simplified shoebox model without interior partitions to maximise cross-ventilation, but real
625 buildings with multiple rooms may have lower cross-ventilation rates, approaching single-
626 sided ventilation. Hence, in more realistic scenarios, NVP for cross-ventilation may resemble
627 that of single-sided ventilation.

628 Additionally, we assume consistent human activities across regions, overlooking any
629 resulting modifications to anthropogenic heat emissions. Local socioeconomic conditions and
630 population density cause large intra-city emission variability. In our study the neighbourhood
631 density accounted for but not the overall inter-city differences in mean city-wide population
632 density. The latter vary from > 2000 per km^2 in Shanghai to around 900 per km^2 in Kunming
633 (Xu et al., 2019). Higher population densities often correspond to increased anthropogenic
634 heat emissions, resulting in higher urban air temperatures that affect NVP. Densely populated
635 neighbourhoods can have greater anthropogenic heat emissions due to increased building
636 energy consumption and traffic-related emissions. Accounting for these variables can impact
637 NVP results. Detailed data can be used to model anthropogenic heat emissions in different
638 neighbourhoods using SUEWS.

639 Our findings should be representative of similar climates and neighbourhoods, but future
640 studies could focus on more detailed information on neighbourhoods in real cities where the
641 variance in NVP might be greater. Existing evaluations suggest that the SUEWS model has
642 acceptable accuracy, although the C_p values should be changed with building geometry. We

643 have only considered buildings and grass in our study and have ignored the impact of trees,
644 which could modify the wind field (Kent et al., 2018) and radiative fluxes (Morrison et al.,
645 2018) and affect the natural ventilation of nearby buildings. Although trees can be modelled
646 in SUEWS and considered as shading objects in EnergyPlus (e.g. Hsieh et al., 2018), to
647 modify wind pressure coefficients on nearby building facets, measurements or CFD
648 simulations are still necessary. Therefore, our approach can be extended with additional data.
649 Additionally, air and noise pollution, which could be high in dense urban areas, may further
650 reduce NVP (as noted in Table 1), but this is beyond the scope of this study and could be
651 considered in future work.

652 **5. Acknowledgement**

653 This work has been funded as part of NERC-COSMA (NE/S005889/1) and ERC urbisphere
654 (855005).

655 **6. Data availability**

656 Information on the data underpinning the results presented here can be found at
657 <https://doi.org/10.5281/zenodo.7802864> (Xie et al., 2023).

658 **7. References**

- 659 Allen, L., Lindberg, F., Grimmond, C.S.B., 2011. Global to city scale urban anthropogenic
660 heat flux: model and variability. *Int. J. Climatol.* 31, 1990–2005.
- 661 Anđelković, A.S., Mujan, I., Dakić, S., 2016. Experimental validation of a EnergyPlus
662 model: Application of a multi-storey naturally ventilated double skin façade. *Energy*
663 *Build.* 118, 27–36.
- 664 ANSI/ASHRAE, 2011. Standard Method of Test for the Evaluation of Building Energy
665 Analysis Computer Programs. Atlanta.
- 666 ANSI/ASHRAE, 2013. Ventilation for Acceptable Indoor Air Quality.
- 667 ASHRAE, 2005. ASHRAE Handbook : Fundamentals. American Society of Heating,
668 Refrigerating and Air-Conditioning Engineers, Atlanta.
- 669 Augusto, B., Roebeling, P., Rafael, S., Ferreira, J., Ascenso, A., Bodilis, C., 2020. Short and
670 medium- to long-term impacts of nature-based solutions on urban heat. *Sustain. Cities*
671 *Soc.* 57, 102122.

- 672 Awbi, H.B., 2003. *Ventilation of Buildings*, Second. ed. Taylor & Francis Group, New York.
- 673 Aynsley, R., 1999. Estimating summer wind driven natural ventilation potential for indoor
674 thermal comfort. *J. Wind Eng. Ind. Aerodyn.* 83, 515–525.
- 675 Boccalatte, A., Fossa, M., Gaillard, L., Menezo, C., 2020. Microclimate and urban
676 morphology effects on building energy demand in different European cities. *Energy*
677 *Build.* 224, 110129.
- 678 CABEE, 2021. *China Building Energy Consumption and Carbon Emission Research Report*.
- 679 Causone, F., 2016. Climatic potential for natural ventilation. *Archit. Sci. Rev.* 59, 212–228.
- 680 Chen, Y., Tong, Z., Malkawi, A., 2017. Investigating natural ventilation potentials across the
681 globe: Regional and climatic variations. *Build. Environ.* 122, 386–396.
- 682 Chen, Y., Tong, Z., Wu, W., Samuelson, H., Malkawi, A., Norford, L., 2019. Achieving
683 natural ventilation potential in practice: Control schemes and levels of automation. *Appl.*
684 *Energy* 235, 1141–1152.
- 685 Cheng, J., Qi, D., Katal, A., Wang, L., Stathopoulos, T., 2018. Evaluating wind-driven
686 natural ventilation potential for early building design.
- 687 Cheng, Z., Li, L., Bahnfleth, W.P., 2016. Natural ventilation potential for gymnasia – Case
688 study of ventilation and comfort in a multisport facility in northeastern United States.
689 *Build. Environ.* 108, 85–98.
- 690 Costanzo, V., Yao, R., Xu, T., Xiong, J., Zhang, Q., Li, B., 2019. Natural ventilation potential
691 for residential buildings in a densely built-up and highly polluted environment. A case
692 study. *Renew. Energy* 138, 340–353.
- 693 Emmerich, S.J., Dols, W.S., Axley, J.W., 2001. *Natural ventilation review and plan for*
694 *design and analysis tools*. National Institute of Standards and Technology, Gaithersburg.
- 695 Faggianelli, G.A., Brun, A., Wurtz, E., Muselli, M., 2014. Natural cross ventilation in
696 buildings on Mediterranean coastal zones. *Energy Build.* 77, 206–218.
- 697 Fernández, M.E., Picone, N., Gentili, J.O., Campo, A.M., 2021. Analysis of the Urban
698 Energy Balance in Bahía Blanca (Argentina). *Urban Clim.* 37, 100856.
- 699 Fumo, N., Mago, P., Luck, R., 2010. Methodology to estimate building energy consumption
700 using EnergyPlus Benchmark Models. *Energy Build.* 42, 2331–2337.
- 701 Germano, M., 2007. Assessing the natural ventilation potential of the Basel region. *Energy*
702 *Build.* 39, 1159–1166.
- 703 Ghiaus, C., Allard, F., Santamouris, M., Georgakis, C., Nicol, F., 2006. Urban environment
704 influence on natural ventilation potential. *Build. Environ.* 41, 395–406.
- 705 Gough, H.L., Barlow, J.F., Luo, Z., King, M.F., Halios, C.H., Grimmond, C.S.B., 2020.
706 Evaluating single-sided natural ventilation models against full-scale idealised
707 measurements: Impact of wind direction and turbulence. *Build. Environ.* 170, 106556.
- 708 Grimmond, C.S.B., Blackett, M., Best, M.J., Baik, J.-J., Belcher, S.E., Beringer, J.,
709 Bohnenstengel, S.I., Calmet, I., Chen, F., Coutts, A., Dandou, A., Fortuniak, K.,
710 Gouvea, M.L., Hamdi, R., Hendry, M., Kanda, M., Kawai, T., Kawamoto, Y., Kondo,
711 H., Krayenhoff, E.S., Lee, S.-H., Loridan, T., Martilli, A., Masson, V., Miao, S., Oleson,
712 K., Ooka, R., Pigeon, G., Porson, A., Ryu, Y.-H., Salamanca, F., Steeneveld, G.J.,
713 Tombrou, M., Voogt, J.A., Young, D.T., Zhang, N., 2011. Initial results from Phase 2 of
714 the international urban energy balance model comparison. *Int. J. Climatol.* 31, 244–272.

- 715 Grimmond, C.S.B., Blackett, M., Best, M.J., Barlow, J., Baik, J.J., Belcher, S.E.,
716 Bohnenstengel, S.I., Calmet, I., Chen, F., Dandou, A., Fortuniak, K., Gouvea, M.L.,
717 Hamdi, R., Hendry, M., Kawai, T., Kawamoto, Y., Kondo, H., Krayenhoff, E.S., Lee,
718 S.H., Loridan, T., Martilli, A., Masson, V., Miao, S., Oleson, K., Pigeon, G., Porson, A.,
719 Ryu, Y.H., Salamanca, F., Shashua-Bar, L., Steeneveld, G.J., Tombrou, M., Voogt, J.,
720 Young, D., Zhang, N., 2010. The International Urban Energy Balance Models
721 Comparison Project: First Results from Phase 1. *J. Appl. Meteorol. Climatol.* 49, 1268–
722 1292.
- 723 Grimmond, C.S.B., Oke, T.R., 1999a. Heat Storage in Urban Areas: Local-Scale
724 Observations and Evaluation of a Simple Model. *J. Appl. Meteorol.* 38, 922–940.
- 725 Grimmond, C.S.B., Oke, T.R., 1999b. Aerodynamic Properties of Urban Areas Derived from
726 Analysis of Surface Form. *J. Appl. Meteorol.* 38, 1262–1292.
- 727 Grimmond, C.S.B., Oke, T.R., Steyn, D.G., 1986. Urban Water Balance: 1. A Model for
728 Daily Totals. *Water Resour. Res.* 22, 1397–1403.
- 729 Grosso, M., 1992. Wind pressure distribution around buildings: a parametrical model. *Energy*
730 *Build.* 18, 101–131.
- 731 Harman, I.N., Finnigan, J.J., 2007. A simple unified theory for flow in the canopy and
732 roughness sublayer. *Boundary-Layer Meteorol.* 123, 339–363.
- 733 Harman, I.N., Finnigan, J.J., 2008. Scalar Concentration Profiles in the Canopy and
734 Roughness Sublayer. *Boundary-Layer Meteorol.* 129, 323–351.
- 735 Havu, M., Kulmala, L., Kolari, P., Vesala, T., Riikonen, A., Järvi, L., 2022. Carbon
736 sequestration potential of street tree plantings in Helsinki. *Biogeosciences* 19, 2121–
737 2143.
- 738 Hensen, J.L.M. (Jan), 1999. Simulation of building energy and indoor environmental quality -
739 Some weather data Issues. *Int. Work. Clim. data their Appl. Eng.* 1–15.
- 740 Hersbach, H., Bell, B., Berrisford, P., Hirahara, S., Horányi, A., Muñoz-Sabater, J., Nicolas,
741 J., Peubey, C., Radu, R., Schepers, D., Simmons, A., Soci, C., Abdalla, S., Abellan, X.,
742 Balsamo, G., Bechtold, P., Biavati, G., Bidlot, J., Bonavita, M., De Chiara, G.,
743 Dahlgren, P., Dee, D., Diamantakis, M., Dragani, R., Flemming, J., Forbes, R., Fuentes,
744 M., Geer, A., Haimberger, L., Healy, S., Hogan, R.J., Hólm, E., Janisková, M., Keeley,
745 S., Laloyaux, P., Lopez, P., Lupu, C., Radnoti, G., de Rosnay, P., Rozum, I., Vamborg,
746 F., Villaume, S., Thépaut, J.N., Muñoz-Sabater, J., Nicolas, J., Peubey, C., Radu, R.,
747 Schepers, D., Simmons, A., Soci, C., Abdalla, S., Abellan, X., Balsamo, G., Bechtold,
748 P., Biavati, G., Bidlot, J., Bonavita, M., Chiara, G., Dahlgren, P., Dee, D., Diamantakis,
749 M., Dragani, R., Flemming, J., Forbes, R., Fuentes, M., Geer, A., Haimberger, L., Healy,
750 S., Hogan, R.J., Hólm, E., Janisková, M., Keeley, S., Laloyaux, P., Lopez, P., Lupu, C.,
751 Radnoti, G., Rosnay, P., Rozum, I., Vamborg, F., Villaume, S., Thépaut, J.N., 2020. The
752 ERA5 global reanalysis. *Q. J. R. Meteorol. Soc.* 146, 1999–2049.
- 753 Hiyama, K., Glicksman, L., 2015. Preliminary design method for naturally ventilated
754 buildings using target air change rate and natural ventilation potential maps in the
755 United States.
- 756 Hsieh, C.-M., Li, J.-J., Zhang, L., Schwegler, B., 2018. Effects of tree shading and
757 transpiration on building cooling energy use. *Energy Build.* 159, 382–397.
- 758 Integrated Environmental Solutions, 2018. MacroFlo calculation methods [WWW
759 Document]. URL <https://help.iesve.com/ve2018/> (accessed 6.30.22).

- 760 Järvi, L., Grimmond, C.S.B., Christen, A., 2011. The Surface Urban Energy and Water
761 Balance Scheme (SUEWS): Evaluation in Los Angeles and Vancouver. *J. Hydrol.* 411,
762 219–237.
- 763 Johnson, M.H., Zhai, Z.J., Krarti, M., 2012. Performance evaluation of network airflow
764 models for natural ventilation, HVAC and R Research.
- 765 Kamal, A., Abidi, S.M.H., Mahfouz, A., Kadam, S., Rahman, A., Hassan, I.G., Wang, L.L.,
766 2021. Impact of urban morphology on urban microclimate and building energy loads.
767 *Energy Build.* 253, 111499.
- 768 Kent, C.W., Lee, K., Ward, H.C., Hong, J.-W., Hong, J., Gatey, D., Grimmond, S., 2018.
769 Aerodynamic roughness variation with vegetation: analysis in a suburban
770 neighbourhood and a city park. *Urban Ecosyst.* 21, 227–243.
- 771 Lam, K.P., Zhao, J., Ydstie, E.B., Wirick, J., Qi, M., Park, J., 2014. An EnergyPlus whole
772 building energy model calibration method for office buildings using occupant behavior
773 data mining and empirical data. In: 2014 ASHRAE/IBPSA-USA Building Simulation
774 Conference. pp. 160–167.
- 775 Li, Y., Li, X., 2015. Natural ventilation potential of high-rise residential buildings in northern
776 China using coupling thermal and airflow simulations. *Build. Simul.* 8, 51–64.
- 777 Lindberg, F., Grimmond, C.S.B., Gabey, A., Huang, B., Kent, C.W., Sun, T., Theeuwes,
778 N.E., Järvi, L., Ward, H.C., Capel-Timms, I., Chang, Y., Jonsson, P., Krave, N., Liu, D.,
779 Meyer, D., Olofson, K.F.G., Tan, J., Wästberg, D., Xue, L., Zhang, Z., 2018. Urban
780 Multi-scale Environmental Predictor (UMEP): An integrated tool for city-based climate
781 services. *Environ. Model. Softw.* 99, 70–87.
- 782 Lindberg, F., Olofson, K.F.G., Sun, T., Grimmond, C.S.B., Feigenwinter, C., 2020. Urban
783 storage heat flux variability explored using satellite, meteorological and geodata. *Theor.*
784 *Appl. Climatol.* 141, 271–284.
- 785 Liu, J., Li, Y., Zhang, C., Liu, Z., 2022. The effect of high altitude environment on diesel
786 engine performance: Comparison of engine operations in Hangzhou, Kunming and
787 Lhasa cities. *Chemosphere* 309, 136621.
- 788 Liu, Y., Stouffs, R., Tablada, A., Wong, N.H., Zhang, J., 2017. Comparing micro-scale
789 weather data to building energy consumption in Singapore. *Energy Build.* 152, 776–791.
- 790 Luo, Z., Zhao, J., Gao, J., He, L., 2007. Estimating natural-ventilation potential considering
791 both thermal comfort and IAQ issues. *Build. Environ.* 42, 2289–2298.
- 792 Magli, S., Lodi, C., Lombroso, L., Muscio, A., Teggi, S., 2015. Analysis of the urban heat
793 island effects on building energy consumption. *Int. J. Energy Environ. Eng.* 6, 91–99.
- 794 Martins, N.R., Carrilho Da Graça, G., 2017. Simulation of the effect of fine particle pollution
795 on the potential for natural ventilation of non-domestic buildings in European cities.
- 796 Mei, S.J., Hu, J.T., Liu, D., Zhao, F.Y., Li, Y., Wang, Y., Wang, H.Q., 2017. Wind driven
797 natural ventilation in the idealized building block arrays with multiple urban
798 morphologies and unique package building density. *Energy Build.* 155, 324–338.
- 799 MoHURD, 2012. Evaluation standard for indoor thermal environment in civil buildings
800 (GB/T50785-2012). Ministry of Housing and Urban-rural Development, P.R. China,
801 Beijing.
- 802 MoHURD, 2015. Design standard for energy efficiency of public buildings (GB50189-2015).
803 Ministry of Housing and Urban-rural Development, P.R. China, Beijing.

- 804 MoHURD, 2016. Code for thermal design of civil building (GB50176-2016). Ministry of
805 Housing and Urban-rural Development, P.R. China, Beijing.
- 806 Morrison, W., Kotthaus, S., Grimmond, C.S.B., Inagaki, A., Yin, T., Gastellu-Etchegorry,
807 J.P., Kanda, M., Merchant, C.J., 2018. A novel method to obtain three-dimensional
808 urban surface temperature from ground-based thermography. *Remote Sens. Environ.*
809 215, 268–283.
- 810 Nicol, F., Humphreys, M., 2010. Derivation of the adaptive equations for thermal comfort in
811 free-running buildings in European standard EN15251. *Build. Environ.* 45, 11–17.
- 812 Oke, T.R., Mills, G., Christen, A., Voogt, J.A., 2017a. *Urban Climates*. Cambridge
813 University Press, Cambridge.
- 814 Oke, T.R., Mills, G., Christen, A., Voogt, J.A., 2017b. *Urban climates*. Cambridge University
815 Press, Cambridge.
- 816 Oropeza-Perez, I., Østergaard, P.A., 2013. Potential of natural ventilation in temperate
817 countries-A case study of Denmark.
- 818 Patil, K.N., Kaushik, S.C., 2015. Study of climatic potential for natural ventilation in
819 buildings for typical Indian cities. *Int. J. Vent.* 13, 369–380.
- 820 Pesic, N., Roset Calzada, J., Muros Alcojor, A., 2018. Natural ventilation potential of the
821 Mediterranean coastal region of Catalonia. *Energy Build.* 169, 236–244.
- 822 Rafael, S., Martins, H., Matos, M.J., Cerqueira, M., Pio, C., Lopes, M., Borrego, C., 2020.
823 Application of SUEWS model forced with WRF: Energy fluxes validation in urban and
824 suburban Portuguese areas. *Urban Clim.* 33, 100662.
- 825 Ramponi, R., Gaetani, I., Angelotti, A., 2014. Influence of the urban environment on the
826 effectiveness of natural night-ventilation of an office building. *Energy Build.* 78, 25–34.
- 827 Royapoor, M., Roskilly, T., 2015. Building model calibration using energy and
828 environmental data. *Energy Build.* 94, 109–120.
- 829 Ryan, E.M., Sanquist, T.F., 2012. Validation of building energy modeling tools under
830 idealized and realistic conditions. *Energy Build.* 47, 375–382.
- 831 Sailor, D.J., 2011. A review of methods for estimating anthropogenic heat and moisture
832 emissions in the urban environment. *Int. J. Climatol.* 31, 189–199.
- 833 Sakiyama, N.R.M., Mazzaferro, L., Carlo, J.C., Bejat, T., Garrecht, H., 2021. Natural
834 ventilation potential from weather analyses and building simulation. *Energy Build.* 231,
835 110596.
- 836 Sun, T., Grimmond, S., 2019. A Python-enhanced urban land surface model SuPy (SUEWS
837 in Python, v2019.2): Development, deployment and demonstration. *Geosci. Model Dev.*
838 12, 2781–2795.
- 839 Sun, T., Järvi, L., Omidvar, H., Theeuwes, N., Lindberg, F., Li, Z., Grimmond, S., 2020.
840 *Urban-Meteorology-Reading/SUEWS: 2020a Release*.
- 841 Sundell, J., Levin, H., Nazaroff, W.W., Cain, W.S., Fisk, W.J., Grimsrud, D.T., Gyntelberg,
842 F., Li, Y., Persily, A.K., Pickering, A.C., Samet, J.M., Spengler, J.D., Taylor, S.T.,
843 Weschler, C.J., 2011. Ventilation rates and health: multidisciplinary review of the
844 scientific literature. *Indoor Air* 21, 191–204.
- 845 Tan, Z., Deng, X., 2017. Assessment of natural ventilation potential for residential buildings
846 across different climate zones in Australia. *Atmosphere (Basel)*. 8, 177.

- 847 Tang, Y., Sun, T., Luo, Z., Omidvar, H., Theeuwes, N., Xie, X., Xiong, J., Yao, R.,
848 Grimmond, S., 2021. Urban meteorological forcing data for building energy simulations.
849 *Build. Environ.* 204, 108088.
- 850 Theeuwes, N.E., Ronda, R.J., Harman, I.N., Christen, A., Grimmond, C.S.B., 2019.
851 Parametrizing horizontally-averaged wind and temperature profiles in the urban
852 roughness sublayer. *Boundary-Layer Meteorol.* 173, 321–348.
- 853 Tong, Z., Chen, Y., Malkawi, A., 2017. Estimating natural ventilation potential for high-rise
854 buildings considering boundary layer meteorology. *Appl. Energy* 193, 276–286.
- 855 Tong, Z., Chen, Y., Malkawi, A., Liu, Z., Freeman, R.B., 2016. Energy saving potential of
856 natural ventilation in China: The impact of ambient air pollution. *Appl. Energy* 179,
857 660–668.
- 858 Toparlak, Y., Blocken, B., Maiheu, B., van Heijst, G.J.F., 2017. A review on the CFD
859 analysis of urban microclimate. *Renew. Sustain. Energy Rev.* 80, 1613–1640.
- 860 TPU, 2007. Aerodynamic database for low-rise buildings. Tokyo, Japan.
- 861 TRNSYS, 2009. TRNSYS 17: Mathematical reference.
- 862 U.S. Department of Energy, 2020a. Chapter 1: Overview. In: *EnergyPlus Version 9.4.0*
863 *Documentation: Engineering Reference*. pp. 20–24.
- 864 U.S. Department of Energy, 2020b. Chapter 13: Alternative modeling processes. In:
865 *EnergyPlus Version 9.4.0 Documentation: Engineering Reference*. pp. 601–705.
- 866 U.S. Department of Energy, 2020c. Chapter 8: Air Heat Balance Manager / Processes. In:
867 *EnergyPlus Version 9.4.0 Documentation: Engineering Reference*. pp. 58–168.
- 868 U.S. Department of Energy, 2020d. Chapter 5: Climate, Sky and Solar/Shading Calculations.
869 In: *EnergyPlus Version 9.4.0 Documentation: Engineering Reference*. pp. 187–224.
- 870 UN, 2015. Paris Agreement.
- 871 UNEP, 2020. 2020 Global Status Report for Buildings and Construction: Towards a
872 Zero-emission, Efficient and Resilient Buildings and Construction Sector. Nairobi.
- 873 van Hooff, T., Blocken, B., 2010. On the effect of wind direction and urban surroundings on
874 natural ventilation of a large semi-enclosed stadium. *Comput. Fluids* 39, 1146–1155.
- 875 van Hooff, T., Blocken, B., Tominaga, Y., 2017. On the accuracy of CFD simulations of
876 cross-ventilation flows for a generic isolated building: Comparison of RANS, LES and
877 experiments. *Build. Environ.* 114, 148–165.
- 878 Wang, B., Malkawi, A., 2019. Design-based natural ventilation evaluation in early stage for
879 high performance buildings. *Sustain. Cities Soc.* 45, 25–37.
- 880 Ward, H.C., Grimmond, C.S.B., 2017. Assessing the impact of changes in surface cover,
881 human behaviour and climate on energy partitioning across Greater London. *Landsc.*
882 *Urban Plan.* 165, 142–161.
- 883 Ward, H.C., Kotthaus, S., Järvi, L., Grimmond, C.S.B., 2016. Surface Urban Energy and
884 Water Balance Scheme (SUEWS): Development and evaluation at two UK sites. *Urban*
885 *Clim.* 18, 1–32.
- 886 Warren, P.R., 1977. Ventilation through openings on one wall only. In: *International*
887 *Conference on Heat and Mass Transfer in Buildings*. Dubrovnik.
- 888 Warren, P.R., Parkins, L.M., 1984. Single-sided ventilation through open windows. In:

- 889 Document - Swedish Council for Building Research. p. 487.
- 890 Wiegels, R., Chapa, F., Hack, J., 2021. High resolution modeling of the impact of
891 urbanization and green infrastructure on the water and energy balance. *Urban Clim.* 39,
892 100961.
- 893 WMO, 2023. Guidance to Measuring, Modelling and Monitoring the Canopy Layer Urban
894 Heat Island, EMS Annual Meeting 2021. Geneva.
- 895 Xie, X., Luo, Z., Grimmond, S., Blunn, L., 2023. Use of wind pressure coefficients to
896 simulate natural ventilation and building energy for isolated and surrounded buildings.
897 *Build. Environ.* 230, 109951.
- 898 Xie, X., Luo, Z., Grimmond, S., Sun, T., Morrison, W., 2022. Impact of inter-building
899 longwave radiative exchanges on building energy performance and indoor overheating.
900 *Build. Environ.* 209, 108628.
- 901 Xiong, J., Yao, R., Grimmond, S., Zhang, Q., Li, B., 2019. A hierarchical climatic zoning
902 method for energy efficient building design applied in the region with diverse climate
903 characteristics. *Energy Build.* 186, 355–367.
- 904 Xu, G., Jiao, L., Yuan, M., Dong, T., Zhang, B., Du, C., 2019. How does urban population
905 density decline over time? An exponential model for Chinese cities with international
906 comparisons. *Landsc. Urban Plan.* 183, 59–67.
- 907 Xu, K., Lu, R., Mao, J., Chen, R., Ke, X.U., Riyu, L.U., Jiangyu, M., Ruidan, C., 2019.
908 Circulation anomalies in the mid–high latitudes responsible for the extremely hot
909 summer of 2018 over northeast Asia. *New pub KeAi* 12, 231–237.
- 910 Yamanaka, T., Kotani, H., Iwamoto, K., Kato, M., 2006. Natural, wind-forced ventilation
911 caused by turbulence in a room with a single opening. *Int. J. Vent.*
- 912 Yan, D., Xia, J., Tang, W., Song, F., Zhang, X., Jiang, Y., 2008. DeST — An integrated
913 building simulation toolkit Part I: Fundamentals. *Build. Simul.* 2008 12 1, 95–110.
- 914 Yang, L., Zhang, G., Li, Y., Chen, Y., 2005. Investigating potential of natural driving forces
915 for ventilation in four major cities in China. *Build. Environ.* 40, 738–746.
- 916 Yang, W., Quan, Y., Jin, X., Tamura, Y., Gu, M., 2008. Influences of equilibrium atmosphere
917 boundary layer and turbulence parameter on wind loads of low-rise buildings. *J. Wind
918 Eng. Ind. Aerodyn.* 96, 2080–2092.
- 919 Yang, X., Zhao, L., Bruse, M., Meng, Q., 2012. An integrated simulation method for building
920 energy performance assessment in urban environments. *Energy Build.* 54, 243–251.
- 921 Yao, R., Li, B., Steemers, K., Short, A., 2009. Assessing the natural ventilation cooling
922 potential of office buildings in different climate zones in China. *Renew. Energy* 34,
923 2697–2705.
- 924 Yin, W., Zhang, G., Yang, W., Wang, X., 2010. Natural ventilation potential model
925 considering solution multiplicity, window opening percentage, air velocity and humidity
926 in China. *Build. Environ.* 45, 338–344.
- 927 Yoon, N., Norford, L., Malkawi, A., Samuelson, H., Piette, M.A., 2020. Dynamic metrics of
928 natural ventilation cooling effectiveness for interactive modeling. *Build. Environ.* 180,
929 106994.
- 930 Zhai, Z. (John), Johnson, M.H., Mankibi, M. El, Stathopoulos, N., 2016. Review of natural
931 ventilation models. *Int. J. Vent.* 15, 186–204.

- 932 Zhang, A., Gao, C., Zhang, L., 2005. Numerical simulation of the wind field around different
933 building arrangements. *J. Wind Eng. Ind. Aerodyn.* 93, 891–904.
- 934 Zhong, H.Y., Sun, Y., Shang, J., Qian, F.P., Zhao, F.Y., Kikumoto, H., Jimenez-Bescos, C.,
935 Liu, X., 2022. Single-sided natural ventilation in buildings: a critical literature review.
936 *Build. Environ.* 212.
- 937

Journal Pre-proof

Highlights

- *SUEWS and EnergyPlus combined to evaluate urban buildings' natural ventilation potential.*
- *Climate, building area fraction and season all influence natural ventilation potential.*
- *Single-sided ventilation can be as effective as cross ventilation in dense urban areas.*

Journal Pre-proof

Declaration of interests

The authors declare that they have no known competing financial interests or personal relationships that could have appeared to influence the work reported in this paper.

The authors declare the following financial interests/personal relationships which may be considered as potential competing interests:

Journal Pre-proof